Received November 23, 2020, accepted December 7, 2020, date of publication December 11, 2020,
date of current version December 28, 2020.

Digital Object Identifier 10.1109/ACCESS.2020.3044088

Miniaturization Trends in Substrate Integrated Waveguide (SIW) Filters: A Review

AMJAD IQBAL[1], (Student Member, IEEE), JUN JIAT TIANG[1], SEW KIN WONG[1], (Member, IEEE), MOHAMMAD ALIBAKHSHIKENARI[2], (Member, IEEE), FRANCISCO FALCONE[3,4], (Senior Member, IEEE), AND ERNESTO LIMITI[2], (Senior Member, IEEE)

[1]Centre for Wireless Technology, Faculty of Engineering, Multimedia University, Cyberjaya 63100, Malaysia
[2]Department of Electronic Engineering, Tor Vergata University of Rome, 00133 Rome, Italy
[3]Department of Electrical Engineering, Public University of Navarre, 31006 Pamplona, Spain
[4]Institute of Smart Cities, Public University of Navarre, 31006 Pamplona, Spain

Corresponding authors: Amjad Iqbal (amjad730@gmail.com) and Mohammad Alibakhshikenari (alibakhshikenari@ing.uniroma2.it)

This work was supported by the Ministerio de Ciencia, Innovación y Universidades, Gobierno de España under Grant RTI2018-095499-B-C31.

ABSTRACT This review provides an overview of the technological advancements and miniaturization trends in Substrate Integrated Waveguide (SIW) filters. SIW is an emerging planar waveguide structure for the transmission of electromagnetic (EM) waves. SIW structure consists of two parallel copper plates which are connected by a series of vias or continuous perfect electric conductor (PEC) channels. SIW is a suitable choice for designing and developing the microwave and millimetre-wave (mm-Wave) radio frequency (RF) components: because it has compact dimensions, low insertion loss, high-quality factor (QF), and can easily integrate with planar RF components. SIW technology enjoys the advantages of the classical bulky waveguides in a planar structure; thus is a promising choice for microwave and mm-Wave RF components.

INDEX TERMS Coupling topology, filters, isolation, metallic via, substrate integrated waveguide (SIW), transmission zero (TZ).

I. INTRODUCTION

RF communication components have gained tremendous attention in recent times. Technology is getting advanced with time and new applications are suggested, explored and successfully deployed. Many applications such as microwave imaging [1], biomedical implantable devices [2], [3], automotive radar applications [4], [5], wearable sensors [6], [7], microwave sensors [8], and wireless networks [9] are recently reported.

The RF front-end of a communication system consists of several active and passive components: it includes mixers, power amplifiers, oscillators, filters, and antennas. Several RF companies are trying to integrate all components into one chip-set to reduce the cost of production and minimize the dimensions [10]. However, there are few components (filters, diplexers, and antennas) that are inconvenient in the chip-set. Because they have large dimensions or their performance reduce when they are integrated into the chip-set. These components exhibit additional space, apart from chip-set, in the package. Normally, more than one chip-set is packed in a single package to form the system-in-package [11]. Planar microstrip technology or coplanar waveguides are used at the lower frequencies; however, transmission and radiation losses in the microstrip or coplanar waveguides limit their applications in the mm-Wave frequencies. Therefore, a promising technology is required to develop the microwave and mm-Wave components at a lower cost and high performance.

Substrate Integrated Waveguide (SIW) technology is considered as one of the suitable choices for developing RF components [12]–[16]. SIWs are considered as quasi-waveguides, developed by two parallel copper sheets with rows of shorting pins on each side to connect the two plates, as shown in Figure. 1. The advantages of a non-planar bulky waveguide are achieved through a planar SIW technology; thus making the non-planar component (waveguide) compatible

The associate editor coordinating the review of this manuscript and approving it for publication was Sotirios Goudos.

for integration with planar circuits, such as a printed circuit board (PCB) and low-temperature co-fired ceramic (LTCC) technology. Dispersion characteristics and field patterns of SIW structure are similar to classical non-planar waveguides. Majority of the classical waveguide properties, such as high power handling capability and high quality factor, exhibits in SIW. One of the biggest advantages of SIW structures is its planar structure and its integration with other planar circuits [17]. Also, integration of more than one chip on one substrate is possible and there is no requirement of transition between the components, thus making the system less lossy. Mounting different chips on one substrate extend the idea of SIP to the system-on-substrate (SoS) [18], and thus is a suitable choice for low-cost, less lossy, compact, and simple microwave and mm-Wave systems.

SIWs were initially recognized as post-wall waveguides [12] or laminated waveguides [13] and then a lot of developments were made to use them for antennas [19], [20], filters [21], [22], couplers, mixers [23], diplexers [24], [25], oscillators [26], [27], and circulators [28]. It is evident that SIW technology is used for all classical waveguide components [19], [28]. The majority of the aforementioned RF components, which are based on SIW technology, work below 30 GHz and few at above 30 GHz [29]–[32]. The limited usage of SIW technology in mm-Wave range frequencies is due to technological complexity in developing. Special attention to material selection is required to develop mm-Wave range components due to its low profile and high losses. Currently, many research groups are trying to overcome these problems to develop high performance SIW RF front-ends at the mm-Wave range.

II. SUBSTRATE INTEGRATED WAVEGUIDE (SIW) STRUCTURES

A. DESIGN GUIDELINES OF SIW STRUCTURES

As discussed in the beginning that SIW is an advanced form of a classical waveguide that can be integrated with a planar dielectric substrate, such as PCB. This emerging SIW structure can be designed with a dielectric material, two parallel metal plates, and a series of vias. The parallel plates cover the dielectric material from top and bottom while the metallic vias are arranged in a series to connect the lower and upper metal plates from the side of the dielectric material, as shown in Figure. 1. The SIW structure is basically a substrate integrated circuit (SIC). The SIC family consists of planar circuits, designed from non-planar circuits such as coaxial lines and classical waveguides. The SIW structures only support the transverse-electric (TE) mode because of the gaps between the metallic via on the side walls of the cavity. The TE mode of the SIW cavity resonator is similar to the classical rectangular waveguide, as shown in Figure. 2. In the majority of scenarios, only TE_{m0} is considered because thickness (h) of the laminate is negligible as compared to the width of SIW.

The authors of [14] and [16] did a detailed discussion on leakage characteristics and wave guidance. The designer of

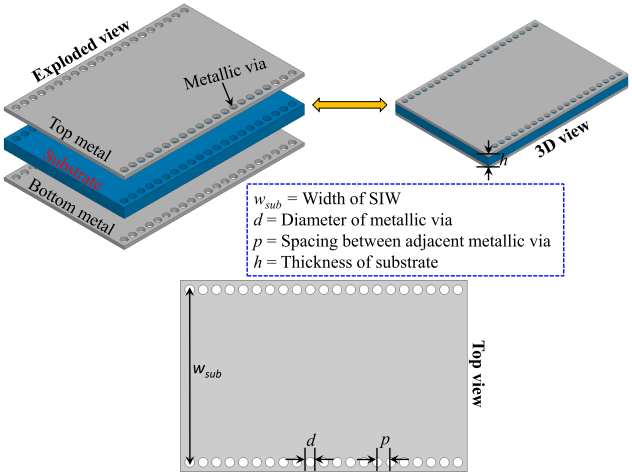

FIGURE 1. The geometry of rectangular SIW structure (top, 3D, and exploded view).

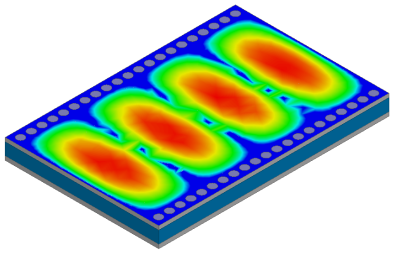

FIGURE 2. Electric fields distribution of the fundamental mode (TE_{10}) of the SIW cavity resonator.

SIW structure must ensure that the SIW cavity resonator is operating at an adequate frequency band and bandgap and leakage losses are negligible. It is known that the top and bottom metal plates are connected through metallic vias from the sides in the SIW components and are always subjected to bandgap losses. If the gap between the two adjacent vias (p) is increased, the majority of the EM fields will no longer remain inside the SIW cavity resonator. As as result, they will propagate through vias and will cause leakage losses. The same phenomenon can be seen if the size of metallic via is reduced. Hence, the SIW structure is not a perfect waveguide and metallic vias dimensions and the gap between adjacent vias may affect the return loss. The following design rules need to be considered to minimize leakage and radiation losses [16].

$$p > d, \tag{1a}$$
$$p/\lambda_c < 0.25, \tag{1b}$$
$$l/k_\circ < 1 \times 10^{-4}, \tag{1c}$$
$$p/\lambda_c > 70.05 \tag{1d}$$

where p is the gap between the adjacent vias, d is the diameter of via, λ_c is the cutoff wavelength, l is the total loss, and $k_\circ$ is the wave number in a vacuum. The condition in Equation. (1a) suggests that diameter (d) of the via must be less than the gap between the adjacent vias (p), so that the SIW structure

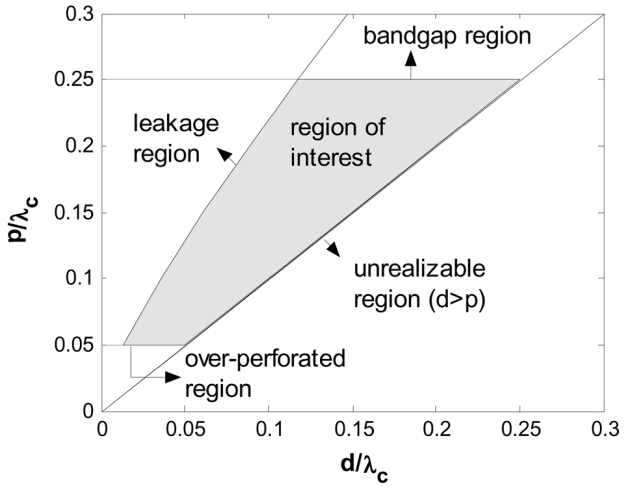

FIGURE 3. Region of interest for the SIW structures as a function of d/λ_c and p/λ_c [16].

is practically designable. Equation. (1b) suggests that the ratio of the gap between the adjacent vias (p) and the cutoff wavelength (λ_c) must be less than 0.25 to avoid bandgap. The leakage loss can be avoided by following the rules suggested in Equation. (1c). Equation. (1d) is desirable but not an essential condition which states that no more than 20 via can be placed per wavelength. Figure. 3 shows the region of interest of the SIW as a function of d/λ_c and p/λ_c [16].

B. OPERATION PRINCIPLES

SIW shows dispersion characteristics and field properties similar to classical non-planar bulky waveguide if the metallic vias are tightly placed with neglected radiation leakage. Classical waveguide supports transverse-electric (TE) and transverse-magnetic (TM) modes while SIW supports only TE mode. The TM mode wave in SIW cannot efficiently transmit because of its inability to form a stable current at sides of metallic vias due to gaps between the metallic vias on the side walls. The electric field distribution of the fundamental SIW mode (TE_{10}) is shown in Figure. 2. It can be noted that the fundamental mode of the SIW structure and the classical waveguide is similar.

As obvious from Figure. 1 that the SIW structure consists of a series of metallic vias at the edges of the structure. The empirical relations between the via's dimensions, SIW's dimensions, and effective width (w_{eff}) of the waveguide are developed in [33], keeping in mind similarities between the classical waveguides and SIW structures. The initial dimensions of the SIW components can be obtained using the equations developed in [33] without the need for rigorous full-wave simulations. The effective with (w_{eff}) of a waveguide is related to the SIW structure parameters in Equation. (2).

$$w_{eff} = w - \frac{d^2}{0.95p} \tag{2}$$

where (w_{eff}) is the effective width of waveguide, w is the width of SIW, $d = 2r$ is the diameter of metallic via, and p is the spacing between the adjacent vias (here p is considered as enough small).

Equation. (2) is further refined in [14] by including d/w ratio because this relation become invalid for larger value of diameter d.

$$w_{eff} = w - 1.08\frac{d^2}{p} + 0.1\frac{d^2}{w} \tag{3}$$

The relation in Equation (3) is valid for $p/d < 3$ and $d/w < 0.5$. Similar type of relation is given as Equation. (4) [34].

$$w = \frac{2w_{eff}}{\pi} cot^{-1}\left(\frac{\pi p}{4w_{eff}} ln\frac{p}{2d}\right) \tag{4}$$

A more accurate calculation of dispersion characteristics and field properties can be performed with the help of electromagnetic (EM) wave simulator such as High-Frequency Structure Simulator (HFSS) and CST Microwave Studio.

C. LOSS MECHANISM

One of the major concerns of the SIW components is to minimize the overall losses, which become more severe at mm-Wave range frequencies. These losses emerge due to conductors (conductor losses), dielectrics (dielectric losses), and gaps between the adjacent vias (leakage losses) [35]–[36]. The losses due to conductors and dielectric material in the SIW components are similar to the corresponding losses in the classical waveguides. Using the classical waveguide equations, the conductor losses can be reduced by increasing the thickness of the substrate because the attenuation constant in a waveguide is inversely related to the thickness of the substrate. The other parameters of SIW component have almost null impact on the conductor losses. The dielectric losses can be minimized by selecting good dielectric material because no other SIW parameter (size and geometry) can affect dielectric loss. The leakage losses which are due to the gaps between the adjacent vias can be minimized by following the rules suggested in Equation (1a-1d). Apart from dielectric, conductor, and leakage losses, surface roughness in the conductors may generate losses in SIW. The surface roughness consideration may be seriously taken into account at higher frequencies. The Quality factors (Q-factors) of SIW, classical non-planar waveguide, and microstrip line is compared in Table. 1. We see from Table. 1 that the classical bulky waveguide has a higher Q-factor followed by SIW and Microstrip line. We know that SIW is made of a low-cost dielectric substrate and the classical bulky waveguide is costly. Thus, SIW shows significant Q-factor at a lower cost and is a suitable choice for low-cost and high Q-factor RF components.

D. BANDWIDTH CONSIDERATIONS

The size of SIW structure and its operational bandwidth is an important part to be considered. The size and bandwidth of SIW structures are limited like classical bulky waveguides. Many approaches have been adopted to enhance the

TABLE 1. Comparison of SIW, Microstrip and Waveguide in terms of Q-factor [37].

Properties	Waveguide	SIW*	Microstrip*
Q-factor	4613	462	42

*Substrate: $\epsilon_r = 2.33$, $\tan\delta = 0.0005$

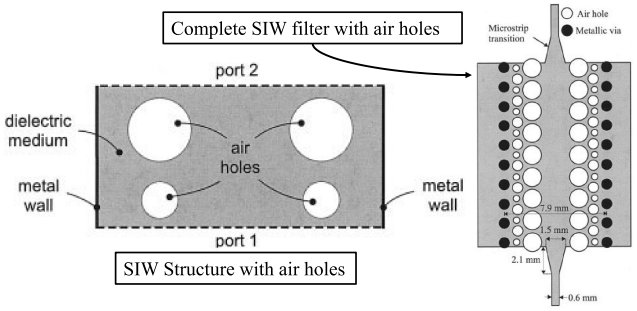

FIGURE 4. Air-filled holes based SIW unit structure and filter [38].

operational bandwidth of the SIW structures. The authors of [38] achieved 40% bandwidth enhancement by loading air-filled holes in the SIW structure. The air-filled holes are periodically distributed over the SIW structure, as shown in Figure. 4. Another approach to increase the bandwidth and reduce the bandgap effects is the ridge SIW [39]. In the ridged SIW structures, the metallic vias are connected with one metallic plate of the SIW while another side of the vias remain open, as shown in Figure. 5. A 37% bandwidth enhancement is achieved by using ridged posts in [39]. The authors of [40] further modified the ridged SIW by introducing the metal sheet below the ridged posts, as shown in Figure. 5. A wide bandwidth of 17 % at a centre frequency of 25 GHz is achieved. The concept of SIW structure with the air-filled holes and the ridged SIW with metal plate is further modified in [41]. The authors of [41] used the SIW with air-filled holes and the ridged SIW with metal plates in one structure to achieve super wideband. The authors successfully achieved a wide bandwidth from 7.1 to 30.7 GHz with the bandwidth improvement of 232 %. The last technique not only increases the operational bandwidth but also reduces the component size. The component with the later technique has a 40 % smaller size than the standard SIW with extremely wide bandwidth.

III. MINIATURIZATION TRENDS IN SIW COMPONENTS

The dimensions of SIW structures are important to be considered in modern compact systems. SIW is still considered as a bulky structure as compared to the microstrip technology. The resonant frequency of TE_{mnp} mode of an SIW having dimensions of $a \times b \times c$ can be calculated using Equation. (5) [42].

$$f_{mnp} = \frac{1}{2\sqrt{\mu\epsilon}}\sqrt{\left(\frac{m}{a}\right)^2 + \left(\frac{n}{c}\right)^2 + \left(\frac{p}{b}\right)^2} \quad (5)$$

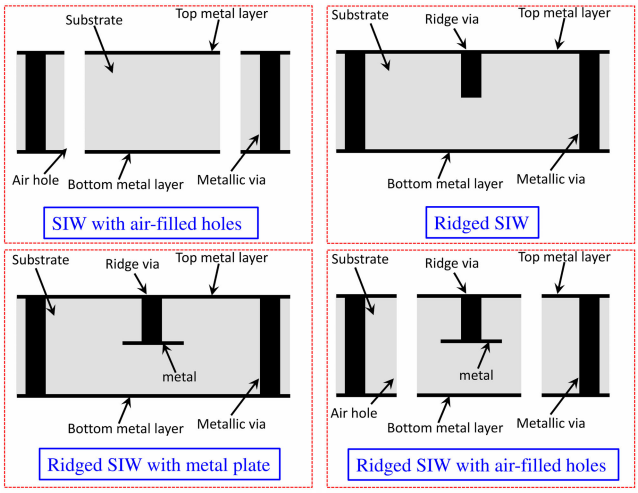

FIGURE 5. SIW with the air-filled holes [38], ridged SIW [39], ridged SIW with the metal sheet [40], and ridged SIW with the air-filled holes for bandwidth enhancement.

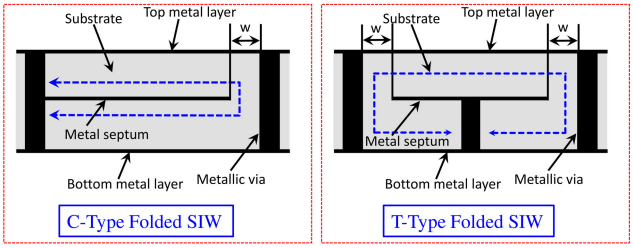

FIGURE 6. Cross section of C- and T-type folded SIW [43]–[44].

where ϵ and μ are permittivity and permeability of the substrate. m,n, and p are the indices of TE mode. a, b, and c represent width, length and thickness of the SIW cavity. Many techniques have been developed in recent times to operate the SIW structures below their fundamental resonant modes. Following are some of the miniaturization techniques.

A. FOLDED SIW

The folded SIW technique for miniaturization is very common in a thin substrate whose thickness is much smaller as compared to its width. There are commonly two types of the folded SIW components (C- and T-type) [43], [44]. This technique sufficiently reduces the SIW dimensions but the losses slightly increase. The cross-section view of both types of folded SIW is shown in Figure. 6.

The authors of [45] used a doubly-folded SIW structures using a low-temperature co-fired ceramic (LTCC) technology. A multilayer structure is adopted to design a quasi-elliptic and Chebyshev filter. Coupling between the vertically SIW resonators is controlled using a U- and L-shaped slots in the middle metallic layer, as shown in Figure. 7. Size reduction of 74% and 88% are noted for quasi-elliptic and Chebyshev filter, respectively.

The authors of [46] used a quadri-folded SIW (QFSIW) for the first time to reduce the SIW dimensions by 89% of the

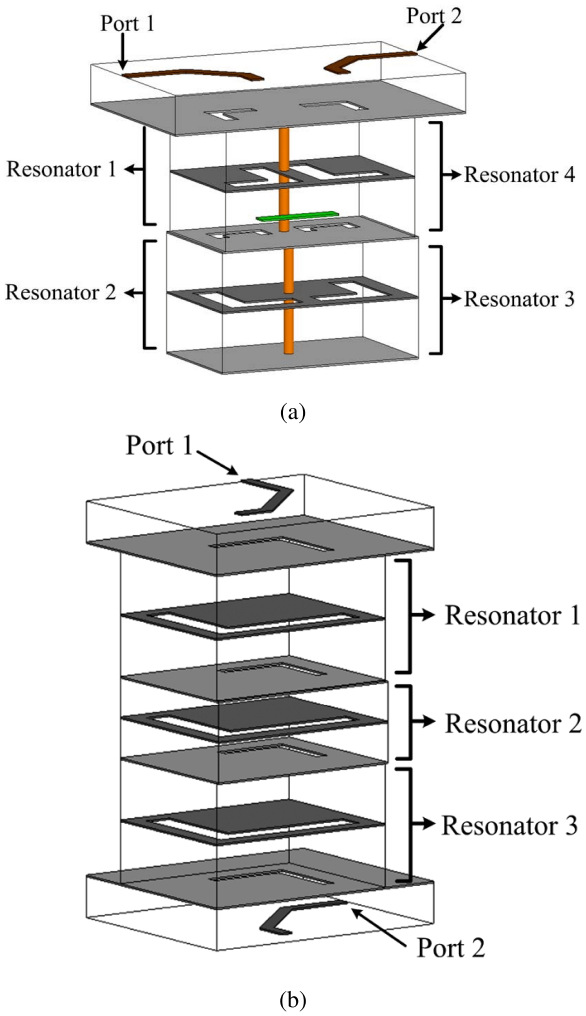

FIGURE 7. Exploded view of the (a) quasi-elliptic, and (c) Chebyshev filter [45].

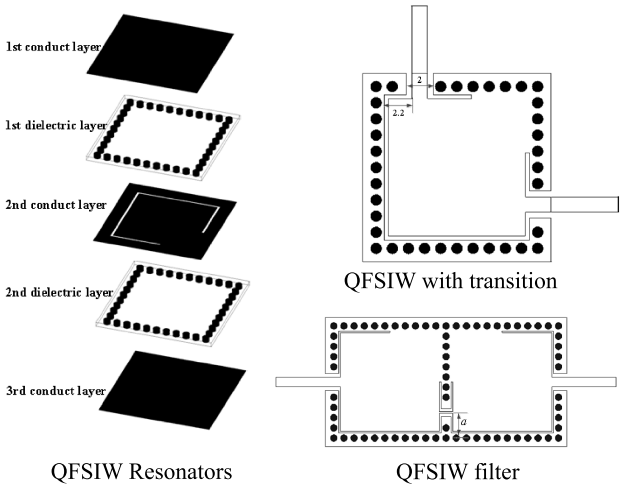

FIGURE 8. Exploded view of the QFSIW resonator, QFSIW resonator with transition, and multilayer QFSIW filter [46].

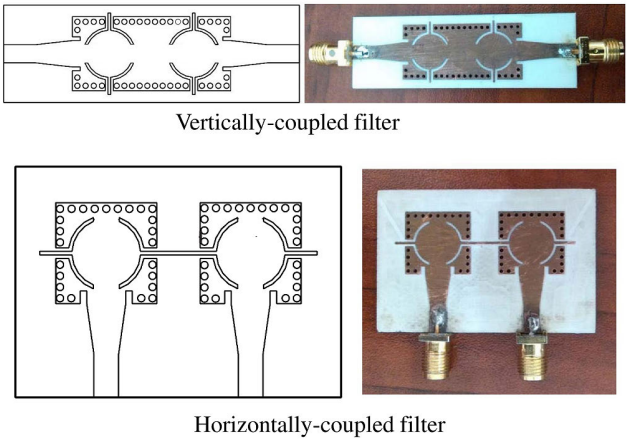

FIGURE 9. Stub-loaded vertically- and horizontally-coupled filters [48].

conventional SIW structures. Figure. 8 shows the exploded view of the QFSIW resonator, QFSIW with transition, and multi-layer QFSIW filter. Coupling between the vertically connected resonators is optimized using a C-shaped slot in the middle copper layer. The concept of such coupling topology and miniaturization technique is verified by designing a fourth-order SIW bandpass filter [46].

B. SLOTS LOADED SIW

Inductive and capacitive loading in an SIW plays important role in shifting the fundamental resonant mode to the lower frequency side. Inductive and capacitive loading may be done either with slots and stubs or adding lumped elements (inductor and capacitor) and other passive components that may induce reactive effects [47].

The authors of [48] reported stubs loaded planar SIW cavity and filters. The purpose of the open-ended stub is to resonate the cavity at the lower frequency than its fundamental resonant frequency. The stubs along with a C-shaped slot is loaded to the SIW cavity in such a way to couple with the magnetic fields. Size reduction of around 61% is achieved using this method. Here, the stubs show inductive behaviour in the SIW cavity. The stub-loaded vertically- and horizontally-coupled filters are shown in Figure. 9 [48].

The authors of [49] reported two frequency tunable multimode filters on the SIW resonators. Each SIW resonator is loaded with an H-shaped slot, as shown in Figure. 10. The H-shaped slot induces capacitive effect on the SIW cavity and hence, TE_{102} mode resonated at a lower frequency than its fundamental frequency. The optimized miniaturized SIW cavity resonator is used to design a horizontally- and vertically-coupled bandpass filters. Frequency tunability in the filters is realized by introducing a varactor diode in the SIW cavity. The varactor diodes are placed to effect both resonant modes to ensure tunabilty.

The authors of [50] designed three different miniaturized dual-mode filters using the SIW technology. Pure rectangular, H- and T-shaped cross-slots are used to induce capacitive effect to the cavity and thus miniaturization is achieved in all

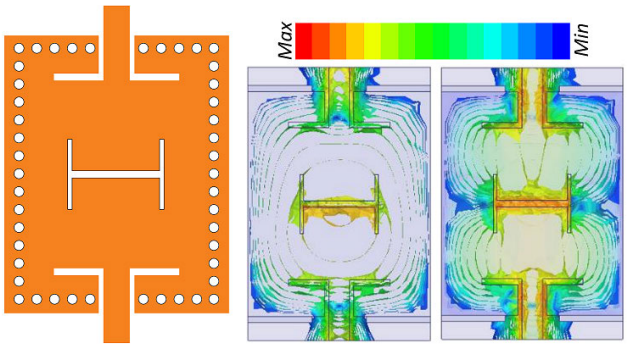

FIGURE 10. H-shaped slot loaded SIW cavity and *E*-fields of the first two resonant modes [49].

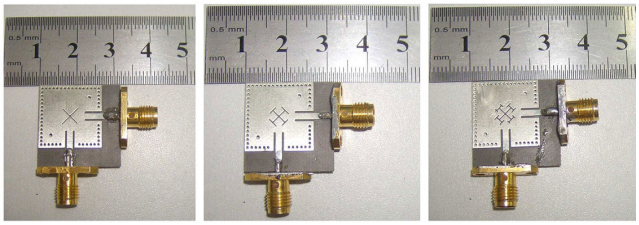

FIGURE 11. Fabricated prototypes of the miniaturized dual-mode SIW filters with the rectangular cross-slots, T-shaped cross-slots, and H-shaped cross-slots [50].

three filters. Size reduction of 22.15%, 30.56%, and 56.25% is achieved by introducing rectangular cross-slots, T-slots, and H-slots, respectively. The fabricated prototypes of all types of the reported filters are shown in Figure. 11.

In [51], the authors reported an ultra-miniaturized SIW cavity resonator for designing a series of bandpass filters. Different techniques are applied to reduce the cavity size. Initially, a square ring slot is introduced to achieve 37% miniaturization. Then, a ramp-shaped slot is used to further increase miniaturization (57% size reduction). Moreover, a rectangular metallic patch is used in the middle layer to further reduce the size. Size reduction of 66% is achieved by introducing a metallic plate in the middle layer. The size of SIW cavity is further reduced (73% miniaturization) by the addition of disconnected vias. The disconnected via further increases the equivalent capacitance of the SIW cavity, and thus more miniaturization is achieved. The same miniaturization techniques are introduced in HMSIW and QMSIW filters to achieve miniaturization of 90% and 95%, respectively. The ultra-miniaturized SIW cavity resonators are used to design multi-standard filters with controllable transmission zeros. A two-pole filter, designed with an ultra-miniaturized SIW cavity resonator, is shown in Figure. 12.

The authors of [52] reported a wideband bandpass filter using the SIW cavity resonator for X-band applications. The reported filter has a fractional bandwidth of 68.4%. It has a centre frequency of 11.7 GHz with a miniaturized overall dimensions of 28.5 $\times$ 16 mm^2. Size reductions and wideband performances are achieved by using open-ended semi-circular slots. The geometry and S-parameter response of the

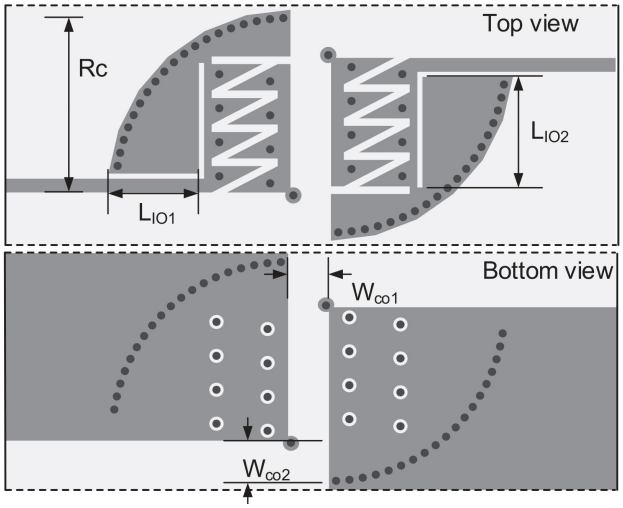

FIGURE 12. The geometry of optimized QMSIW filter ($W_{CO1} = 4$, $R_C = 18$, $L_{I02} = 10.9$, $W_{CO2} = 4.4$, and $L_{IO1} = 8.9$ [unit = mm]) [51].

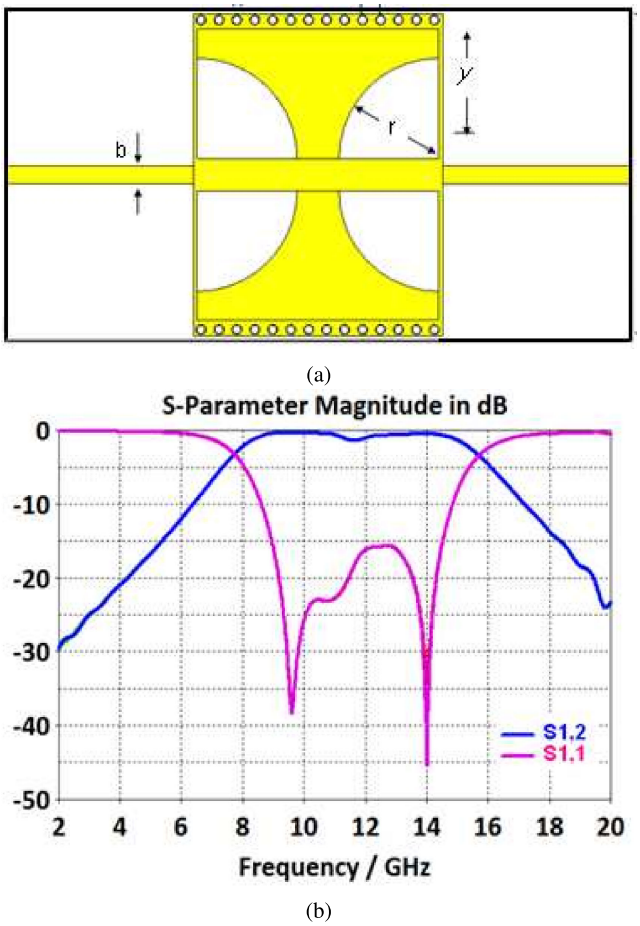

FIGURE 13. (a) The geometry of miniaturized wideband filter, and (b) S-parameter response [52].

reported filter is shown in Fig. 13. Size reduction of around 70% is achieved using this technique.

The authors of [53] reported dual-band bandpass filters on a miniaturized E-shaped slot-loaded SIW cavity resonator.

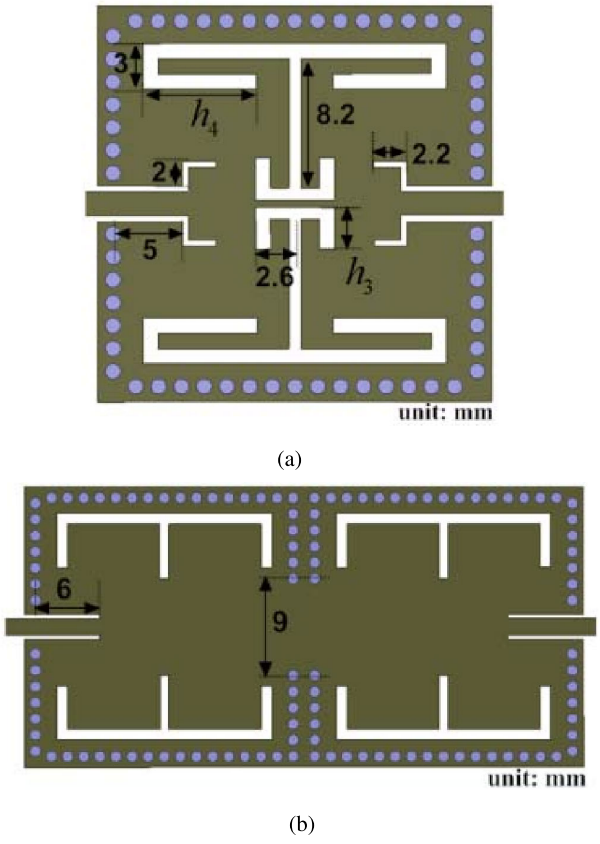

FIGURE 14. Filter design using E-shaped slotted SIW cavity resonator (a) one cavity, and (b) two cavities [53].

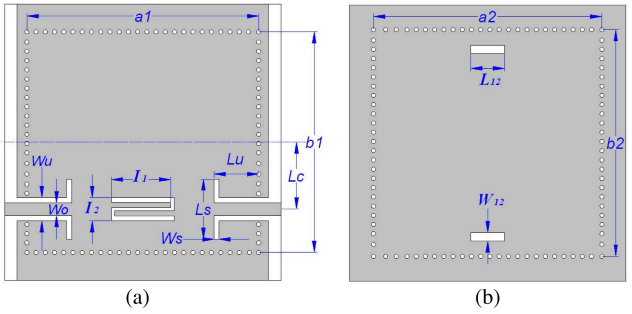

FIGURE 15. The geometry of multilayer filter (a) top copper layer ($a1 = 13.75$, $b1 = 13.05$, $L_c = 3.96$, $L_s = 3.6$, $L_u = 2.75$, $l_1 = 3.55$, $W_o = 0.75$, $W_s = 0.3$, $W_u = 1.4$, and $l_2 = 1.4$ [unit = mm]), and (b) middle metal layer ($a2 = 13.5$, $b2 = 13.45$, $L_{12} = 2.05$, and $W_{12} = 0.5$ [unit = mm]) [54].

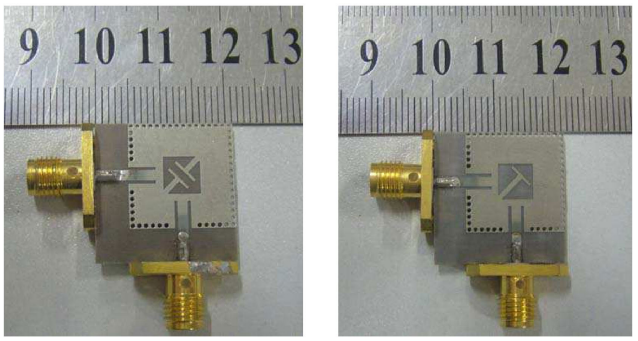

FIGURE 16. Fabricated prototype of the dual-mode SIW cavity filter loaded with two diagonal T-shaped stubs and one diagonal T-shaped stub [55].

Miniaturization in the SIW cavity resonator is achieved by loading an E-shaped slot on the edges of the SIW cavity resonator. The position of an E-shaped slot is optimized so as to couple with the magnetic fields of the resonant modes, resulting in size reduction of the SIW cavity resonator. The miniaturized SIW cavity resonator is verified by using it for designing dual-band filters. Size reduction of around 33% is achieved using this technique. The geometry of an E-shaped slotted single-cavity filter and dual-cavity filter is shown in Figure. 14.

In [54], a low-profile multi-layer filter is reported. The reported filter is designed using dual-mode SIW cavity resonators. The resonators are coupled vertically with one another using two rectangular slots in the middle copper layer. The rectangular slots control the electric and magnetic coupling among the resonators. The proposed filter is not much superior in miniaturization than the conventional dual-resonator filters. However, it has exceptional control over the transmission zeros and selectivity. The geometry (top and middle copper layer) of the dual-resonator filter is shown in Figure. 15.

The authors of [55] reported a dual-mode filter on a single SIW cavity resonator. Miniaturization in the SIW cavity resonator is achieved by designing a T-shaped open-ended stub in the square-slot at the centre of the SIW cavity. The fundamental resonant frequency is lowered from 9.46 GHz to 6.88 GHz by applying this technique, and thus 27% size reduction is achieved. The fabricated prototype of the dual-mode filters are designed on a Rogers 5880 laminate, as shown in Figure. 16.

C. SLOW-WAVE TECHNIQUE

One of the major techniques for reducing the circuit size of SIW components is slow-wave technique [56]. The slow-wave technique in SIW components can be incorporated on a double-layer topology. It requires two substrates, where the metallic vias on the edge of the structure are connected between the bottom copper layer of the lower substrate and upper copper layer of the top substrate. Moreover, the internal metallic vias are connected between the bottom copper layer of the lower substrate and the top region of the lower substrate. The 3-D and side view of the slow-wave SIW structure are shown in Figure. 17. The separation of the electric and magnetic fields leads to a slow-wave effect, thus causes miniaturization. It is demonstrated in [56] that the longitudinal dimensions of the SIW cavity is reduced by >40% of the conventional SIW cavity resonator. Moreover, more than 40% reduction in the phase velocity and traversal dimensions is observed. All the comparisons are performed by designing a classical SIW cavity resonator at 9.3 GHz and then the slow-wave technique is implemented in the same SIW cavity resonator.

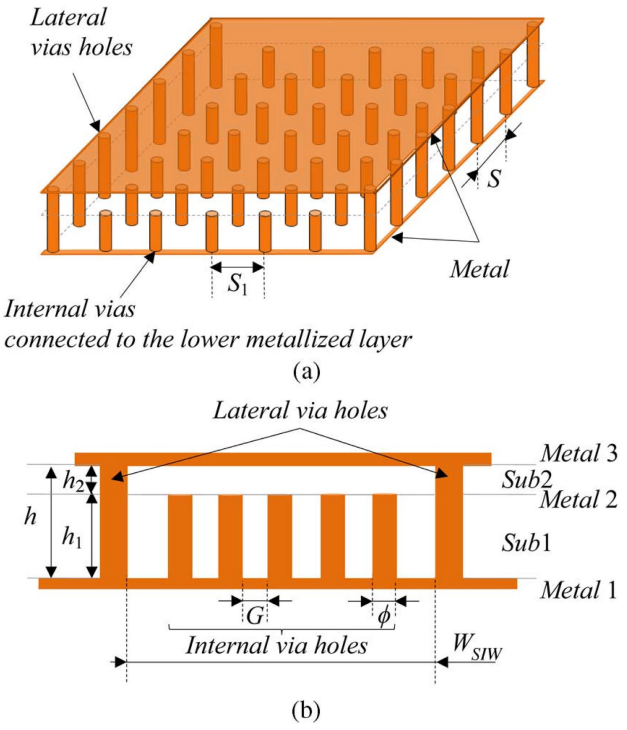

FIGURE 17. The geometry of the slow-wave SIW structures (a) 3-D view, and (b) side view [56].

In [57], a slow-wave structure technique is applied for the design of compact and miniaturize SIW inductive post and iris filters. This technique is basically a dual-layer technique, which maintains high isolation of the electric and magnetic fields. Therefore miniaturization is maintained. By applying this technique, the insertion losses of both filters are improved. The insertion loss is enhanced by 0.23% in the inductive post filter and 7.53% in the iris filter. Moreover, the circuit size of the inductive post filter is miniaturized by 6.36%. In the same way, the circuit size of the iris filter is miniatured by 72.72%. In addition, both filters maintain high quality factors (918.5 in the iris slow-wave SIW filter and 755.15 in the inductive post slow-wave SIW filter) in miniaturized conditions. Therefore, the signal in these two filters travel faster and thus the group delay is enhanced. A comparison between the iris slow-wave SIW filter and the inductive post slow-wave SIW filter is given in [57], which shows that the iris slow-wave filter is better. The geometries of the iris slow-wave SIW filter and inductive post slow-wave SIW filter is shown in Figure 18.

In [58], a miniaturized 5th-order SIW filter is designed using slow-wave technique. The designed filter has a centre frequency of 11 GHz, 3-dB bandwidth of 900 MHz and return loss lower than 12 dB. A two-layer structure is used to implement slow-wave technique. The internal metallic-via holes are connected with the bottom copper-layer of the lower substrate which tends the electric field to reside inside the upper substrate. Moreover, using these metallic vias, the magnetic field reside inside the lower substrate. Therefore the isolation

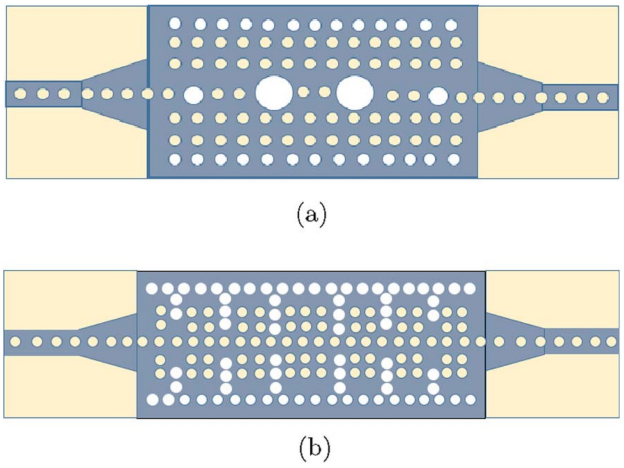

FIGURE 18. SIW Filters with slow-wave technique (a) inductive post filter, and (b) iris filter [57].

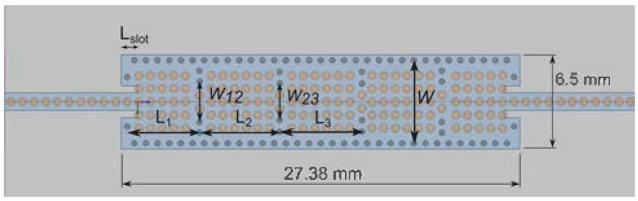

FIGURE 19. The geometry of the slow-wave 5th-order SIW filter [L_1 = 4.97, W_{12} = 2.78, L_2 = 5.5, W_{23} = 2.50, W = 5.7, L_{slot} = 1.1, and L_3 = 5.66 (unit = mm)] [58].

between the electric and magnetic fields is maintained. As a result, three times smaller dimensions (70% miniaturization factor), as compared to conventional classical SIWs, are achieved. Moreover, fractional bandwidth of the filter is improved from 5.95% to 8%. It is observed that the insertion loss of the slow-wave SIW filter is more than that of the classical SIW filter. It is suggested to use a low-loss substrate and air-filled cavities to maintain the lower insertion losses. The geometry of the slow-wave 5th-order SIW filter is shown in Figure. 19.

In [59], slow-wave technology is adopted in the SIW cavity resonator to design miniaturized SIW filters. The slow-wave effect is generated by periodic metallic vias in the SIW cavity resonator. As a result, the cavity size is reduced, the bandwidth and return loss is improved. A bandpass filter with the centre frequency of 11 GHz and 3-dB bandwidth of 1000 MHz is designed to verify the concept. In addition, the slow-wave SIW filter has 60% lower dimensions. Moreover, the optimization time is significantly reduced by segmentation and curve fitting techniques. The fabricated prototype of the slow-wave SIW filter is shown in Figure. 20.

The authors of [60] designed an SIW-based bandpass filter at 12 GHz. The reported filter covers the X-band and has a 3-dB operational bandwidth of 1000 MHz. Miniaturization in the filter is achieved through the slow-wave technique. It is observed that the filter length (area) is reduced by 22.79% (40.39%) as compared to the conventional SIW

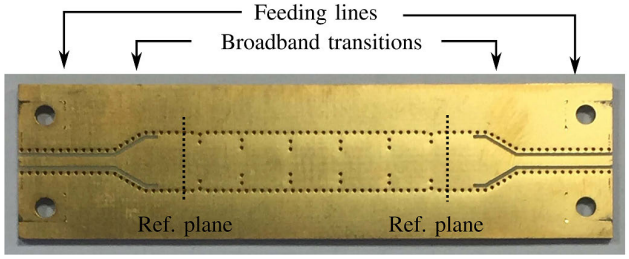

FIGURE 20. Fabricated prototype of the slow-wave SIW filter [59].

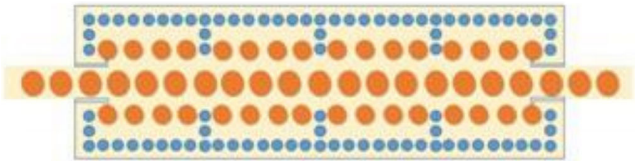

FIGURE 21. Schematic (bottom view) of the slow-wave SIW filter [60].

filter. Moreover, the selectivity and out-of-band rejection is improved with increase in the order of filter. The schematic (bottom view) of the filter is shown in Figure. 21.

D. STEPPED-IMPEDANCE METAMATERIAL STRUCTURES

Just like other miniaturization techniques, stepped-impedance metamaterial structures (SIMMS) are also used in SIW components for miniaturization [61]–[62]. The working principles of SIMMS are based on evanescent mode propagation [63]. It states that an electric dipole (above the waveguide) can be used to achieve a passband below the cutoff frequency of the waveguide. By loading SIMMS on the SIW components, a negative permittivity is expected. Based on its negative permittivity, SIMMS can be consider as an electric dipole [63]. Therefore, a passband below the cutoff frequency is possible by loading SIMMS to the SIW cavity resonator. The authors of [63] designed a HMSIW-based filter and diplexer. The circuit size of the filter is reduced by incorporating SIMMS in the HMSIW cavity resonator. The geometry of the SIMMS based HMSIW filter is shown in Figure. 22. Initially, an SIW filter is designed which is converted to the HMSIW, achieving 50% miniaturization. Then the filter dimensions are further reduced by incorporating SIMMS in it. It reduces the filter dimensions by more than 50% of the HMSIW filter. In fact, the dimensions of SIMMS-based HMSIW filter is reduced by 75% as compared to the conventional SIW cavity filter. Finally, a high-isolated diplexer is developed by combining the two filters with unique frequencies.

In [64], a HMSIW cavity resonator based bandpass filter is designed. Then, miniaturization is achieved by loading a uniform split-ring resonator (USRR) and SIMMS over the resonator. In fact, the SIMMS increases the capacitance and inductance value of the resonator. As a result, the centre frequency shifts towards the lower frequency side and miniaturization is achieved. It achieves miniaturization of around 33% as compared to the conventional HMSIW filter. The reported

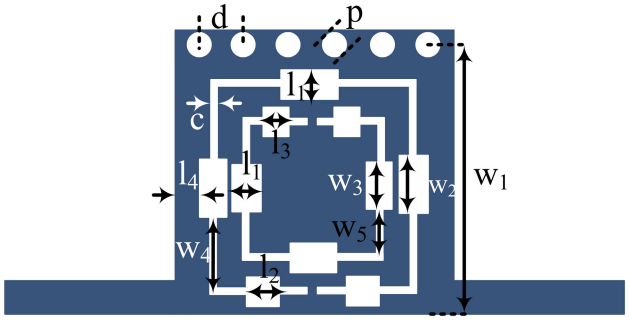

FIGURE 22. Schematic (bottom view) of the SIMMS-based HMSIW filter [63].

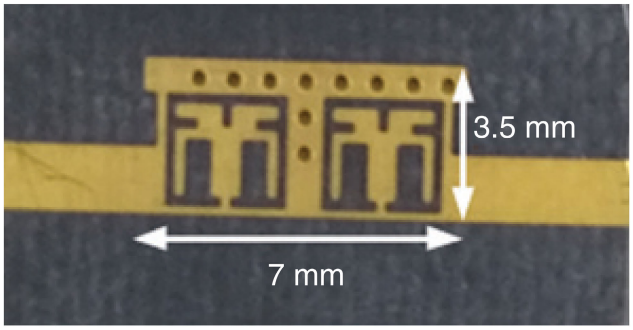

FIGURE 23. Fabricated prototype of the SIMMS-based SIW filter [64].

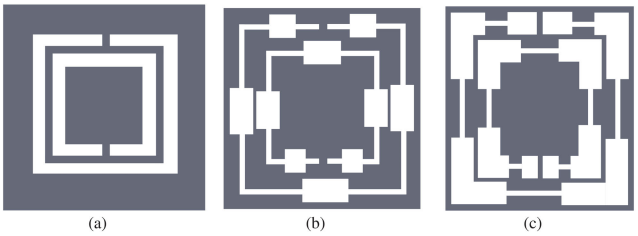

FIGURE 24. (a) Conventional split-ring resonator, (b) type-1 SIMMS, and (c) type-2 SIMMS [65].

filter has a centre frequency of 8.6 GHz, inter-resonator coupling of 0.099 and fractional bandwidth of 10%. Furthermore, it has a lower insertion loss value of 1.53 dB. Besides its compactness, it also has a wide stop-band rejection. It has a stop-band up to 24 GHz with a rejection level of 20 dB.

The authors of [65] reported two types of SIMMS to miniaturize SIW-based filters. The SIMMS geometries are obtained by modifying the conventional split-ring resonator, as shown in Figure. 24. The uniform slots in the conventional split-ring resonator are modified to design stepped-impedance slots. Therefore, the electrical length of the slots significantly increases. As a result, sufficient miniaturization is achieved as compared to the conventional split-ring resonator. The concept of miniaturization is verified by designing and developing different bandpass filters. All filters are designed on a 0.508 mm thick RO4003C laminate. The miniaturization factor of 63% and 60% is achieved for type-1 and

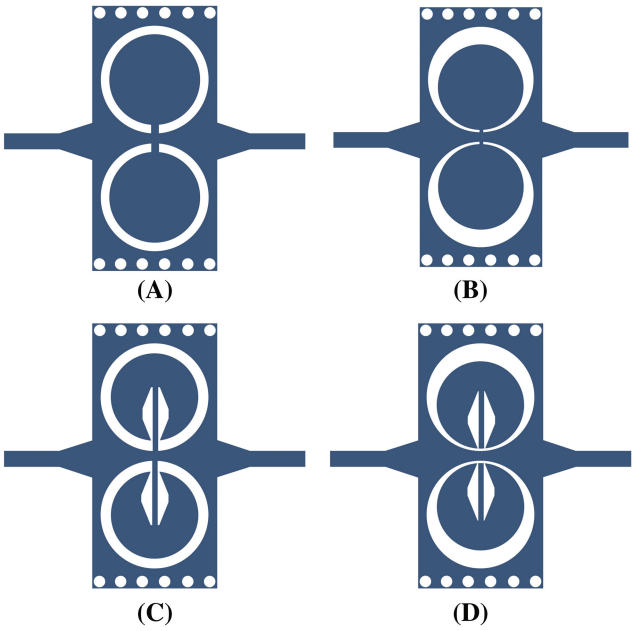

FIGURE 25. SIW filters (a) conventional split-ring resonator (type-1), (b) quasi-SIMMS (type-2), (c) G-shaped split-ring resonator (type-3), and (d) G-shaped SIMMS (type-4) [66].

type-2 SIMMS-based SIW filters, respectively. It is observed that the reported filters have suitable selectivity and have multiple TZs on both sides of the passband. Both filters have the fractional bandwidths of more than 9% with an insertion loss of 1.2 dB (type-1) and 1.2 dB (type-2). The SIMMS are implemented on the upper copper-layer of the SIW cavity resonator. Therefore, radiation can be expected from the upper copper-layer of the resonator. The forward radiation loss is also calculated for all types of filters. It is shown that those filters have radiation loss of less than 0.0012. Thus, it confirms that the SIMMS has less impact on the radiation loss. In addition, the in-band return loss is lower than 15 dB in all filters.

In [66], different types of SIMMS geometries are reported to develop miniaturized SIW-based filters and diplexers. Figure. 25 shows different geometries (conventional split-ring resonator [type-1], quasi-SIMMS [type-2], G-shaped split-ring resonator [type-3], and G-shaped SIMMS [type-4]), which can be used to develop miniaturized SIW components (filters and diplexers). Initially, a conventional split-ring resonator is designed using uniform circular slots. Then, the same split-ring resonator is modified to develop a G-shaped SIMMS. It is observed that the G-shaped SIMMS reduces the circuits (filters and diplexers) sizes by 69% as compared to the conventional SIW circuits. A highly selective filter, having multiple TZs on both sides of the passband, is designed at 5.8 GHz for WLAN band. It has an insertion loss of 1.1 dB and a fractional bandwidth of 7.8%. Furthermore, the in-band return loss of the filter is lower than 21 dB. The filter cover the overall circuit area of $0.169\lambda_g \times 0.08\lambda_g = 0.013\ \lambda_g^2$. Moreover, the group delay in the passband is less than 2.2 ns. There are several slots loaded on the upper copper-layer of

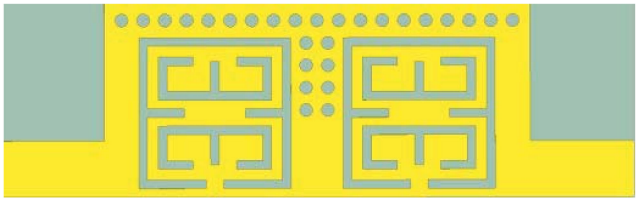

FIGURE 26. Diagram (top view) of the SIMMS-based HMSIW filter [67].

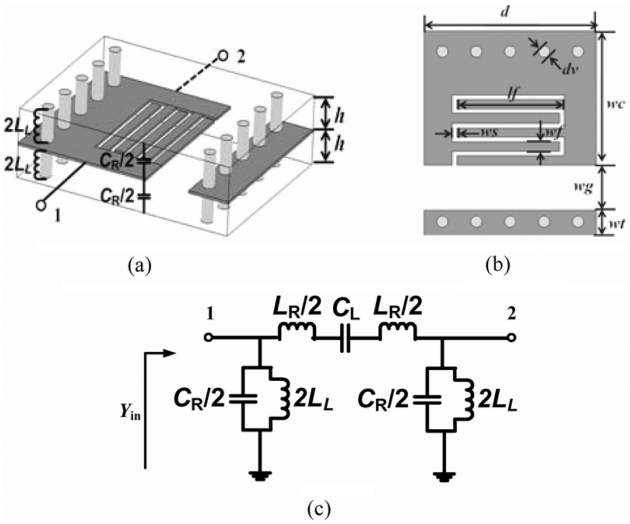

FIGURE 27. CLRH structure based folded-SIW (a) 3D view, (b) top view, and (c) equivalent circuit model [68].

the resonator. Therefore, radiation can be expected from the upper copper-layer of the resonator. The forward radiation loss can be be computed from Equation (6) [66]. It is shown that the reported filter has a radiation loss of less than 0.0012. Thus, it confirms that the SIMMS has a less impact on the radiation loss. Finally, a two-channels diplexer is designed at 4.41 and 5.83 GHz. It has the insertion loss values of 2.2 dB at 4.41 GHz and 2.5 dB at 5.83 GHz. The return loss values are lower than 14 dB in both channels. Moreover, an isolation of more than 30 dB is achieved.

$$R_{loss} = 1 - |S_{11}|^2 - |S_{21}|^2 \tag{6}$$

In the above equation [Equation (6)], R_{loss} is the forward radiation loss due to the slots in the resonator, S_{11} is the reflection coefficient of the filter and S_{21} is the transmission coefficient of the filter.

The authors of [67] designed a novel and miniaturized HMSIW filter. Dual-iris coupling topology is used to couple the resonators together to form a bandpass filter. Miniaturization (around 10% as compared to the conventional HMSIW cavity resonator) in the HMSIW cavity resonator is achieved by loading the nested SIMMS to the HMSIW cavity resonator. A second-order bandpass filter is realized using the miniaturized cavity resonator. It is developed on a 0.508 mm thick RT/duroid 5880 laminate. It has the centre frequency of

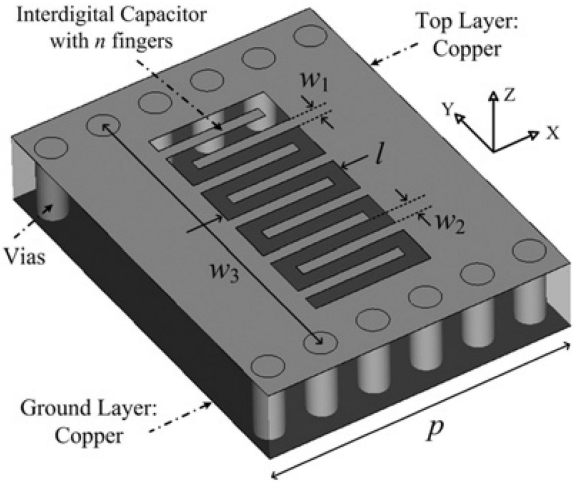

FIGURE 28. Unit-geometry of CLRH-based SIW cavity resonator [72].

6.35 GHz and a 3-dB bandwidth of 690 MHz. In addition, the in-band return loss is lower than 14 dB. Moreover, a TZ on the higher-frequency side of the passband is observed, which improves selectivity of the filter. Diagram (top view) of the SIMMS-based HMSIW filter is shown in Figure. 26.

E. COMPOSITE LEFT/RIGHT-HANDED STRUCTURES

In recent times, left-handed (LH) and right-handed (RH) metamaterial or composite left/right-handed (CLRH) structures have received significant recognition because of their numerous advantages [68]–[71]. The advantages include lower losses, lower circuit dimensions and high quality factor.

In [68], a novel folded-SIW resonator is designed to incorporate CLRH structures. The CLRH structures are used to shift the cut-off frequency of the resonator to the lower frequency side. As a result, miniaturization is achieved. Initially, a folded-SIW cavity resonator was adopted to reduce the circuit size by 50%. CLRH structure based folded-SIW cavity resonator is shown in Figure. 27. Later on, CLRH structures are introduced to reduce the circuit size by 80% as compared to the folded-SIW cavity resonator. The concept of CLRH structures is further verified by designing different *H*-plane filters. A fourth-order filter is designed with a centre frequency of 5.3 GHz and a fractional bandwidth of 6.2%. *H*-plane slots are used to couple the four resonators together. The in-band return loss of the filter (fourth-order filter) is less than 15 dB. The simulated (measured) insertion loss is 3.5 dB (4.3 dB). It has the quality factor of 176. The optimized fourth-order filter is fabricated on a 0.508 mm thick RT/duroid 5880 laminate.

In [72], a novel CLRH structure based SIW cavity resonator is reported, as shown in Figure. 28. The circuit size of the SIW-based cavity resonator is reduced by loading the CLRH structure. The CLRH structure behaves as a series capacitance and shunt inductance, thus achieves CLRH functionality. The CLRH structure generates the resonance below the cutoff frequency of the SIW resonator. After optimizing

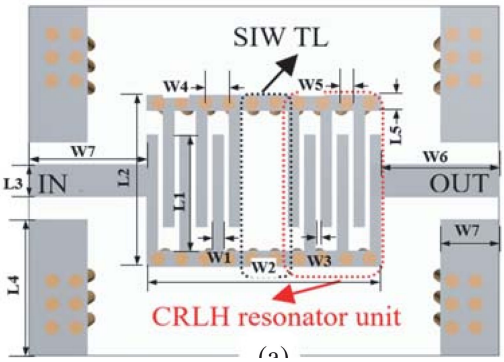

FIGURE 29. CLRH-based SIW cavity filter [73].

the unit-geometry of CLRH-based SIW cavity resonator, low-sized first-order antennas are designed. Then, the same resonators are used to design second-order and third-order bandpass filters. A 1.27 mm thick RT/duroid 5880 laminate is used to develop the antennas and bandpass filters. The reported antenna has a resonance at 7.75 GHz with peak gain (efficiency) of 4.5 dBi (91.3%). The circuit size of the antenna is reduced by 31.41% as compared to the conventional SIW antenna. A second-order bandpass filter is also designed with a fractional bandwidth of 6.5% at a centre frequency of 6.11 GHz. It has the insertion loss of 1.59 dB and return loss of less than 17.2 dB. The in-band group delay is less than 1.2 ns. Furthermore, a third-order filter is also designed with a centre frequency of 6.06 GHz and a fractional bandwidth of 6.4%. It has the insertion loss of 1.86 dB and return loss less than 15.4 dB. The in-band group delay is less than 1.9 ns. The quality factor of 50 and 101 is noted for the second- and third-order bandpass filter, respectively. The third-order filter has a relatively good out-of-band rejection as compared to the second-order filter. A miniaturization of around 45% is achieved in both filters.

In [73], a CLRH-based SIW bandpass is reported. The filter is designed by using CLRH structures in combination with SIW technology. The geometry of CLRH-based SIW filter is shown in Figure. 29. Miniaturization in the conventional SIW cavity resonator is achieved through the addition of CLRH structures. The reported filter has a centre frequency of 5.8 GHz and 3-dB bandwidth of 200 MHz. It has an insertion loss of 2.3 and overall circuit area of $0.19\lambda_\circ \times 0.14\lambda_\circ$. Moreover, the in-band return loss of the filter is lower than 10 dB and group delay is 0.77 ns.

In [74], a sawtooth CLRH-based SIW cavity resonator is designed. Miniaturization is achieved by using a high dielectric constant substrate (RT/duroid 6010 with a dielectric constant of 10.2) and sawtooth-shaped slots instead of conventional spiral CLRH structure. It is demonstrated that the sawtooth slots provide about 50% increase in the capacitance value as compared to the conventional CLRH structure. These slots (sawtooth) enhance the left-handed and right-handed properties of the CLRH structures. The lower-sized resonator is used for a second-order bandpass filter. A second-order bandpass filter is designed with a centre frequency of

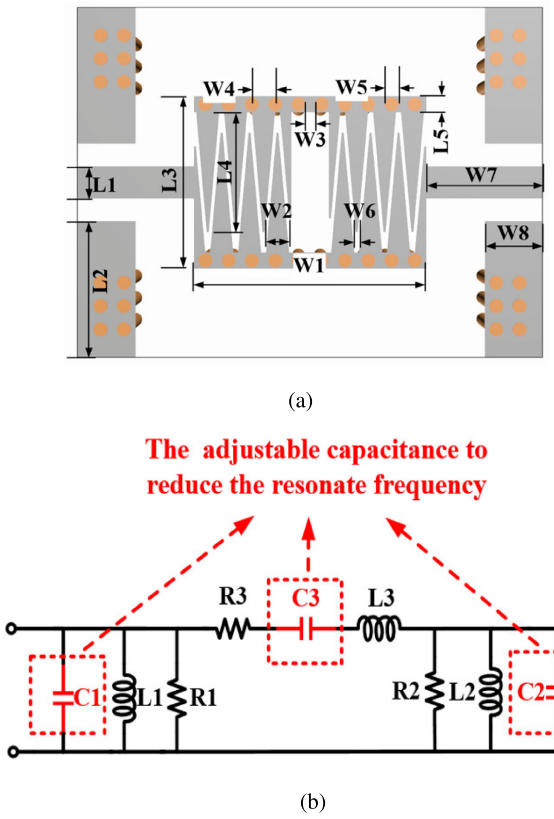

FIGURE 30. (a) The geometry of sawtooth CLRH-based SIW bandpass filter, and (b) Lumped element equivalent circuit model [74].

3.35 GHz and 3-dB bandwidth of 200 MHz. Furthermore, the insertion loss of the filter is less than 2.4 dB in the passband. Moreover, the in-band return loss of the filter is lower than 37 dB and group delay is 1.4 ns. The overall circuit area of the filter is $0.12\lambda_\circ \times 0.09\lambda_\circ$. The geometry and lumped element equivalent circuit model is shown in Figure. 30.

F. SUB MODES OF FULL-MODE SIW

Electric field patterns of the fundamental mode (TE_{101}) in a conventional full-mode circular-SIW cavity resonator, half-mode SIW (HMSIW), quarter-mode SIW (QMSIW), eighth-mode SIW (EMSIW), sixteenth-mode SIW (SMSIW), and thirty-two-mode SIW (HMSIW) are shown in Figure. 31. The solid line is considered as an electrical wall and the dashed line as a magnetic wall, as shown in Figure. 31. Symmetrical planes of A-A1, B-B1, C-C1, and D-D1 in Figure. 31a are considered as magnetic walls. The full-mode SIW cavity resonator can be realized as a half-mode SIW (HMSIW) by cutting it along the symmetrical A-A1 line, as shown in Figure. 31b. We see that the field pattern of the fundamental mode remains unchanged and 50% size reduction is achieved. The HMSIW cavity can be converted to the quarter-mode SIW (QMSIW) by cutting the HMSIW cavity along the O-B line, as shown in Figure. 31c. 50% miniaturization can be achieved by the QMSIW cavity as compared to the HMSIW. The QMSIW can be reduced to the

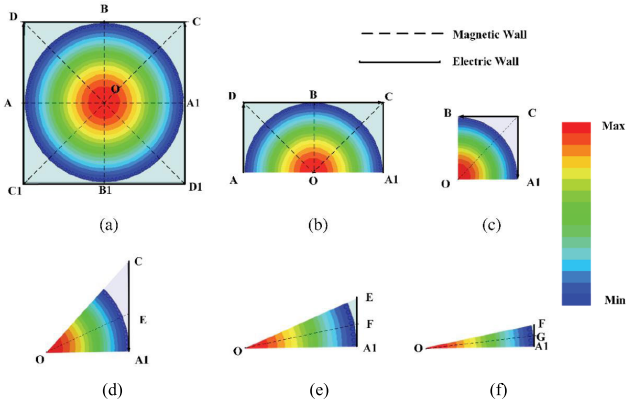

FIGURE 31. Field distribution of the circular SIW cavity resonator (a) full-mode, (b) half-mode, (c) quarter-mode, (d) eighth-mode, (e) sixteenth-mode, and (f) thirty-second-mode [75].

eighth-mode SIW (EMSIW) by cutting the QMSIW cavity along the O-C line, as shown in Figure. 31d. The electric field pattern of the fundamental SIW cavity mode and the EMSIW cavity resonator remains identical with almost the same resonant frequency. The EMSIW cavity can be converted to sixteenth-mode SIW (SMSIW) and thirty-two-mode (TMSIW) by cutting the EMSIW cavity along the O-E and O-F line respectively, as shown in Figure. 31e-f. It is clear that the SMSIW cavity can be reduced by a factor of 15/16 and the TMSIW is reduced by a factor of 31/32. In the same way, the TMSIW cavity resonator can be reduced to sixty-fourth mode SIW (SFMSIW) by cutting along the O-G line. The SFMSIW cavity can be reduced by a factor of 63/64. The resonant frequency and electric field pattern of the fundamental mode remains the same for all sub-modes of the conventional full-mode SIW cavity resonator.

1) HALF-MODE SIW (HMSIW)

In [76], a dual-band HMSIW tunable filter is reported. Each passband can be tuned independently (the first passband can be tuned from 3.26 to 3.47 GHz, and the second passband can be tuned from 5.47 to 6.13) using varactor diodes. The dual-band filter is designed by coupling two dual-mode HMSIW cavity resonators. The dual-mode HMSIW cavity resonators are coupled using E-shaped slots. The coupling between two cavities is adjusted using dimensions of the E-shaped slots, as shown in Figure. 32a. The reported HMSIW cavity resonator exhibits the same field distribution as the conventional full-mode SIW cavity resonator for TE_{101} mode and TE_{102} mode. A rectangular slot from an open-ended side of the HMSIW is designed to further reduce the dimensions of the cavity resonator and to assist in the production of the second resonant mode.

The authors of [77] reported a frequency-reconfigurable multi-layer HMSIW filter with an improved upper stopband performance. The passband, bandwidth and TZs can be tuned by controlling the reverse bias voltage of the varactor diodes. The passband can be tuned between 1.21 and 1.72 GHz

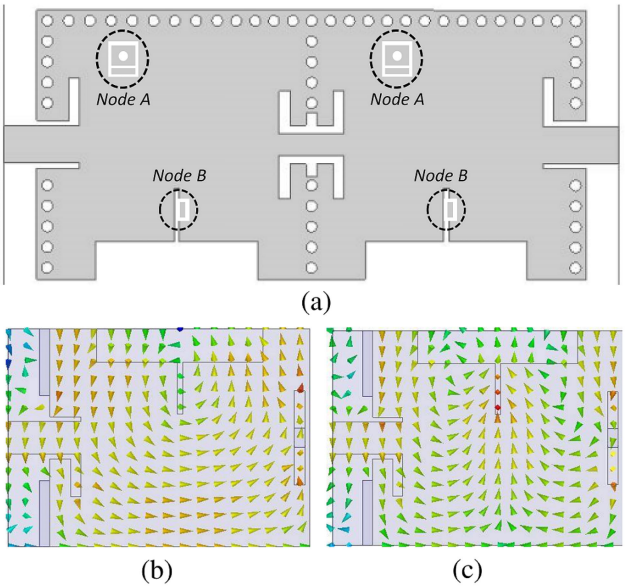

FIGURE 32. (a) The geometry of dual-mode dual-band HMSIW filter, (b) H-fields distribution of the TE_{101} mode, and (c) H-fields distribution of the TE_{102} mode [76].

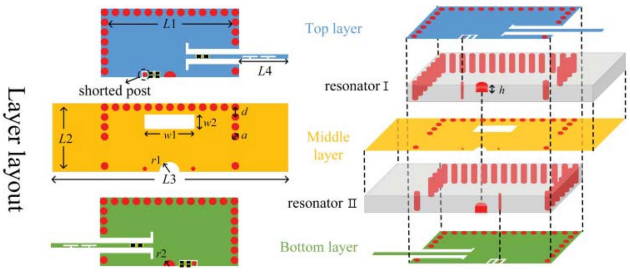

FIGURE 33. The geometry (layer layout and cross view) of tunable HMSIW filter [77].

and a 3-dB bandwidth can be tuned from 62 to 101 MHz. A semi-circle and rectangular slots are used to adjust the coupling between the lower and upper HMSIW cavity resonators. A T-shaped slotted microstrip transmission line is used to suppress the TE_{102} mode, thus achieving an improved upper stopband performance. The reported filter has a 50% lower size than a conventional SIW filter. The reported filter has even less dimensions than the horizontally-coupled SIW filters because of its vertical coupling. The geometry (layer layout and cross view) of the tunable HMSIW filter is shown in Figure. 33.

2) QUARTER-MODE SIW (QMSIW)

The authors of [78] reported a low profile comb-shaped slotted QMSIW cavity resonator and its application in designing a bandpass filter. The QMSIW has reduced dimensions of 75% than the conventional full-mode SIW cavity resonators, and the majority of researchers stop achieving 75% miniaturization. In the reported work, comb-shaped slots are used to induce more capacitance effect to further reduce

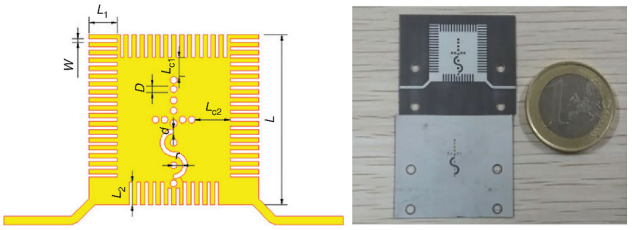

FIGURE 34. The geometry and fabricated prototype of QMSIW filter [$L = 15$, $W = 0.3$, $L_1 = 2.5$, $L_2 = 2$, $r = 0.8$, $L_{c1} = 1.7$, $L_{c2} = 3$, $D = 0.6$, and $d = 0.4$ (unit = mm)] [78].

the dimensions (around 86% miniaturization as compared to the conventional full-mode SIW cavity resonator). Four miniaturized QMSIW cavity resonators are used to design a bandpass filter. The coupling effect between the resonators is controlled through the parameters L_{c1}, L_{c2}, and dimensions of the S-shaped slot. Furthermore, the dimensions of the S-shaped slot are optimized to improve out-of-band rejection. The S-shaped slot is also responsible to generate source-load coupling and thus produces TZs on either side of the passband. The designed filter has four poles with two TZs on both sides of the passband. The geometry and fabricated prototype of the comb-shaped slotted QMSIW filter is shown in Figure. 34.

In [79], a miniaturized quad-poles wideband filter is designed on the QMSIW cavity resonators. The QMSIW cavity resonator has a 75% size reduction as compared to the conventional full-mode SIW. Further miniaturization in the reported QMSIW cavity resonator is achieved by etching the meandered H-shaped slot. The wideband filter is designed by coupling the four QMSIW cavity resonators. The H-shaped slots on each cavity are designed to suppress the higher-order modes and thus enhance the upper stopband performance. The quality factor can be controlled by position and impedance of the microstrip transmission line. Higher selectivity is ensured by sufficiently coupling all resonators and enabling source-load coupling. Coupling between the resonators can be controlled by area coverage of the metallic via between the resonators. The centre frequency and bandwidth of the filter are dependent on the length of the H-shaped slot ($l1$). Moreover, the bandwidth is also dependent on the position of the length of the H-shaped slot ($l1$) without affecting the centre frequency. The optimized dimensions are selected to balance the bandwidth, centre frequency, and stopband suppression. The overall filter occupies dimensions of $0.225\lambda_g \times 0.293\lambda_g \times 0.0027\lambda_g$ (where λ_g is the guided wavelength at 3.25 GHz). The reported filter has the FBW of 21.2% with the insertion loss of less than 1.02 dB and return loss of less than 17 dB. The stopband suppression from 4.02 GHz to 12.63 GHz is seen with a rejection level of higher than 25 dB. The geometry (top and 3D view) of the quad-pole wideband QMSIW filter is shown in Figure. 35.

G. EIGHTH-MODE SIW (EMSIW)

In [80], an ultra-miniaturized bandpass filter is designed. The geometry of the reported filter is shown in Figure. 36.

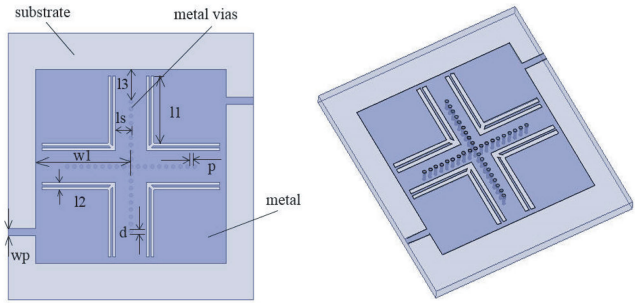

FIGURE 35. Top and 3D view of the quad-poles wideband QMSIW filter [l3 = 3, ls = 1.3, w1 = 10.4, l2 = 0.8, wp = 0.78, p = 0.77, l1 = 8, and d = 0.4 (unit = mm)] [79].

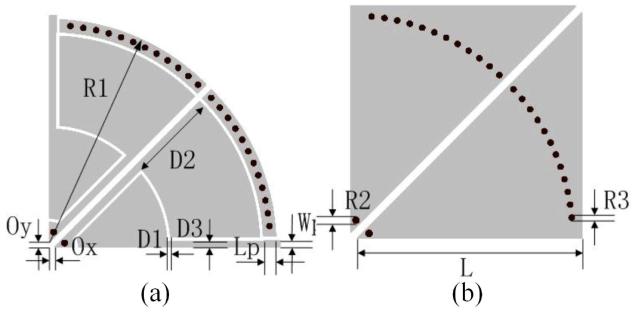

FIGURE 36. The geometry of the filter (a) top view and (b) bottom view [80].

The bandpass filter is designed on a miniaturized EMSIW cavity resonator. Inductive and capacitive sections are added to the EMSIW cavity resonator to further reduce the physical dimensions of the circuit. A miniaturization factor of 98.8% is achieved by combining couple of miniaturization techniques. The miniaturization factor of 87.5% is achieved by adopting the EMSIW cavity resonator instead of the full-mode cavity resonator. The miniaturization factor is further enhanced (98.8%) by the addition of inductive and capacitive sectors to the EMSIW cavity resonator. Apart from miniaturization, couple of techniques are applied to suppress the higher-order modes. The suppression of the higher-order modes is desirable to improve the upper stopband performance. Two transmission zeros are generated in the stopband using the CPW and circular ring as a feeding method.

A multi-layer and low-profile bandpass filter is reported in [81]. The geometry and coupling topology of the filter is shown in Figure. 37. The bandpass filter is composed of two vertically coupled miniaturized EMSIW cavity resonators. A large capacitance is added to the middle copper layer through slot loading. The large capacitance in the middle copper layer achieves additional miniaturization. The reported filter has controllable transmission zeros. The reported circuit achieve more than 87.5 % miniaturization as compared to the conventional full-mode SIW cavity resonator.

H. SIXTEENTH-MODE SIW (SMSIW)

The authors of [82] reported a compact and dual-pole bandpass filter using SMSIW cavity resonators. Each SMSIW cavity resonator excites the fundamental TM_{01} mode. The optimal coupling between the two resonators is achieved by

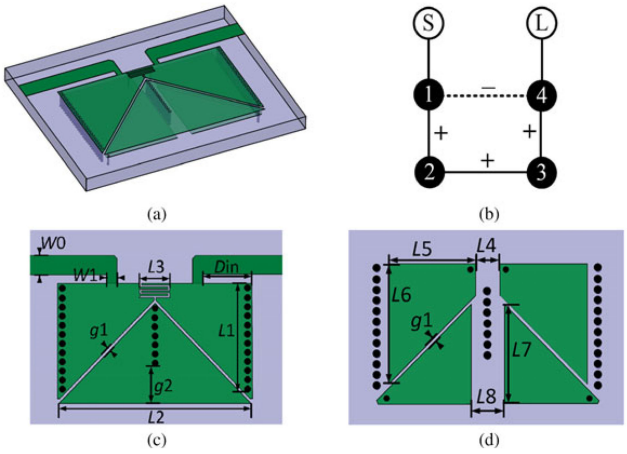

FIGURE 37. Capacitively-loaded EMSIW filter (a) 3D view, (b) coupling topology, (c) top layer and (d) middle layer [81].

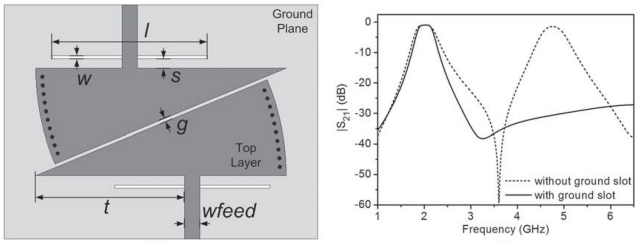

FIGURE 38. Top view of the reported dual-pole bandpass filter and S-parameter results of the filter [82].

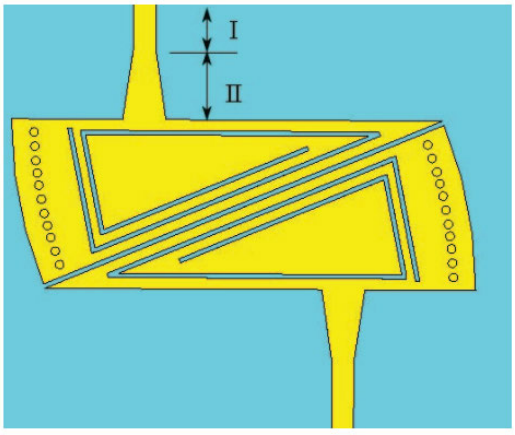

FIGURE 39. The geometry of the helical slot-loaded SMSIW cavity based bandpass filter [83].

properly adjusting the gap between the cavity resonators. The higher-order mode (TM_{02} mode) is suppressed by etching a rectangular slot on the ground plane below the transmission line. It can be noted from Figure. 38 that the rectangular slot is responsible for suppressing the TM_{02} mode. The suppression level of more than 18 dB is achieved from the passband to 8 GHz. The reported geometry achieved a miniaturization factor of 93.75 % as compared to the conventional full-mode SIW cavity.

TABLE 2. Comparison of different miniaturization techniques in SIW filters (FBW = fractional bandwidth, NA = not available, and IL = insertion loss).

Ref	Miniaturization Technique	Size Reduction (%)	Order	Centre Frequency (GHz)	FBW (%)	IL (dB)	Selectivity
[45]	Double-Folded SIW-1	75	3	30	2.9	0.1	Low
	Double-Folded SIW-2	88	3	60	10	0.1	Low
[46]	Quadri-folded SIW	89	4	3.2	9.3	1.6	Medium
[48]	Stub loading	61	2	5.2	5	1	Low
[49]	Slot loading	NA	4	2.7	22.6	1.5	Medium
[50]	Rectangular slots	22.15	2	14.09	9.1	0.79	High
	T-shaped slots	30.56	2	13.30	8.12	0.96	High
	Cross-slots	56.25	2	12.25	6.86	1.21	High
[52]	Open-ended slots	70	2	11.7	68.4	0	Low
[53]	E-shaped slot	33	2	3.6, 6.4	8.2,6.7	1.2	High
[55]	T-shaped stub	27	2	6.88	2.62	1.12	Low
[57]	Slow-wave (Iris filter)	72.2	2	7.79	6.62	0.45	Medium
[58]	Slow-wave	70	5	11	8	3.2	Low
[59]	Slow-wave	60	5	11	9.1	1.9	Medium
[62]	SIMMS	33	2	8.6	10	1.53	High
[65]	SIMMS	70	2	1.8	10.5	1.2	Medium
[66]	SIMMS	69	2	5.8	7.8	1.1	Medium
[68]	CLRH	80	4	5.3	6.2	1.5	Medium
[72]	CLRH	45	2	6.11	6.5	1.59	High
[74]	CLRH	NA	2	3.35	5.7	2.4	Medium
[75]	TMSIW	96.87	2	2.45	36.7	0.25	Medium
[78]	QMSIW+slots	86	2	6.3	5	2	High
[79]	QMSIW	75	4	3.25	21.2	1.02	High
[80]	EMSIW+reactive sectors	98.8	2	0.69	10.2	1.25	High
[81]	EMSIW	87.5	4	1.02	8.35	1.55	High
[82]	SMSIW	93.75	2	2.05	7	1.2	Medium
[83]	SMSIW+helical slot	95	2	2.3	14	1	Low
[84]	SMSIW+CSRR	93.75	2	2.45	8.2	0.9	Medium

In [83], an ultra-compact bandpass filter is reported. The geometry of the filter is shown in Figure. 39. The reported filter consists of two SMSIW resonators. Each SMSIW resonator is loaded with helical slots for additional miniaturization. Using helical slots in the SMSIW resonators, a miniaturization factor of 10 % is achieved as compared to the SMSIW cavity resonators. The performance of the reported filter is analysed with and without the helical slots. As a results, the passband of the filter is shifted to 2.3 GHz from 2.5 GHz. It is worth noticing that the dominant mode of the cavity (TM_{01} mode) remained the same in the ultra-miniaturized cavity.

The authors of [84] reported a dual-resonator bandpass filter. The resonators of the bandpass filter are based on SMSIW cavities. Miniaturization of around 93.75 % is achieved by adopting the SMSIW cavity resonator as compared to the

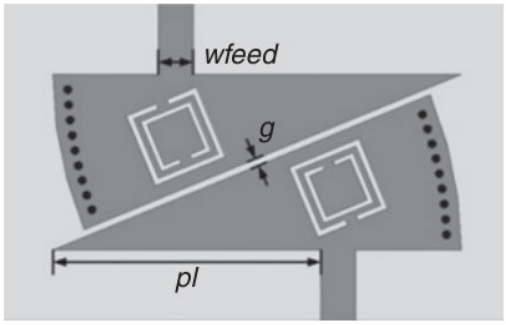

FIGURE 40. Top view of the reported complementary split-ring resonator loaded SMSIW filter [84].

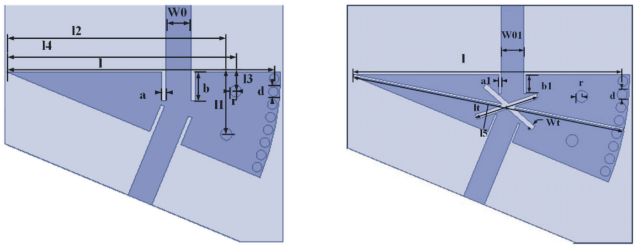

FIGURE 41. Top view of the filter (a) SMSIW and (b) TMSIW [75].

conventional full-mode SIW cavity resonator. A complementary split-ring resonator is loaded to each SMSIW cavity resonator to further reduce the dimensions. The optimal coupling between the two resonators is achieved by properly adjusting the gap between the cavity resonators. The reported filter has the insertion loss of 0.9 dB and the return loss lower than 10 dB.

I. THIRTY-SECOND-MODE SIW (TMSIW)

The authors of [75] reported SMSIW and TMSIW bandpass filters. Miniaturization of 93.75 % and 96.87 % is achieved by adopting the SMSIW and TMSIW cavity resonator instead of the conventional full-mode SIW cavity resonator. In TMSIW filter, both cavities are capacitively coupled.

To sum up, comparison of the different miniaturization techniques in SIW filters is presented in Table. 2.

IV. CONCLUSION

This article presented a detailed review of the state-of-the-art technological advancements and miniaturization techniques in SIW filters. Differences and similarities between the classical waveguides and the SIW structure are discussed. The advantages of SIW components concerning the other technologies are presented. Detailed design guidelines, operation principles, loss mechanism, and bandwidth consideration for SIW cavity resonator are explained. Different approaches to reduce the circuit sizes are explained in details. It is observed that the hybrid miniaturization techniques are preferable for compact devices. The hybrid techniques include a combination of sub-modes with the other miniaturization techniques, such as reactive loading (hybrid technique = sub-modes+reactive loading).

REFERENCES

[1] M. Shahidul Islam, M. Samsuzzaman, G. K. Beng, N. Misran, N. Amin, and M. T. Islam, "A gap coupled hexagonal split ring resonator based metamaterial for S-band and X-band microwave applications," *IEEE Access*, vol. 8, pp. 68239–68253, 2020.
[2] A. Basir and H. Yoo, "A stable impedance-matched ultrawideband antenna system mitigating detuning effects for multiple biotelemetric applications," *IEEE Trans. Antennas Propag.*, vol. 67, no. 5, pp. 3416–3421, May 2019.
[3] A. Basir, A. Bouazizi, M. Zada, A. Iqbal, S. Ullah, and U. Naeem, "A dual-band implantable antenna with wide-band characteristics at MICS and ISM bands," *Microw. Opt. Technol. Lett.*, vol. 60, no. 12, pp. 2944–2949, Dec. 2018.
[4] U. Naeem, D. Zelenchuk, V. Fusco, M. Keaveney, M. O'Shea, and J. Breslin, "Automotive RADAR front-end with added target estimation in elevation plane," in *Proc. IEEE Int. Symp. Antennas Propag. USNC-URSI Radio Sci. Meeting*, Jul. 2019, pp. 937–938.
[5] U. Naeem, V. Fusco, M. Keaveney, M. O'Shea, and J. Breslin, "Low cost 3D printed Fabry–Perot antenna for automotive radar applications," in *Proc. 49th Eur. Microw. Conf. (EuMC)*, Oct. 2019, pp. 512–514.
[6] A. Iqbal, A. J. Alazemi, and N. Khaddaj Mallat, "Slot-DRA-based independent dual-band hybrid antenna for wearable biomedical devices," *IEEE Access*, vol. 7, pp. 184029–184037, 2019.
[7] A. Iqbal, A. Smida, A. J. Alazemi, M. I. Waly, N. Khaddaj Mallat, and S. Kim, "Wideband circularly polarized MIMO antenna for high data wearable biotelemetric devices," *IEEE Access*, vol. 8, pp. 17935–17944, 2020.
[8] A. Iqbal, A. Smida, O. Saraereh, Q. Alsafasfeh, N. Mallat, and B. Lee, "Cylindrical dielectric resonator antenna-based sensors for liquid chemical detection," *Sensors*, vol. 19, no. 5, p. 1200, Mar. 2019.
[9] R. C. Daniels and R. W. Heath, "60 GHz wireless communications: Emerging requirements and design recommendations," *IEEE Veh. Technol. Mag.*, vol. 2, no. 3, pp. 41–50, Sep. 2007.
[10] A. M. Niknejad and H. Hashemi, *mm-Wave Silicon Technology: 60 GHz Beyond*. Cham, Switzerland: Springer, 2008.
[11] M. P. Gaynor, *System-in-package RF Design and Applications*. Norwood, MA, USA: Artech House, 2006.
[12] J. Hirokawa and M. Ando, "Single-layer feed waveguide consisting of posts for plane TEM wave excitation in parallel plates," *IEEE Trans. Antennas Propag.*, vol. 46, no. 5, pp. 625–630, May 1998.
[13] H. Uchimura, T. Takenoshita, and M. Fujii, "Development of a 'laminated waveguide,'" *IEEE Trans. Microw. Theory Techn.*, vol. 46, no. 12, pp. 2438–2443, Dec. 1998.
[14] F. Xu and K. Wu, "Guided-wave and leakage characteristics of substrate integrated waveguide," *IEEE Trans. Microw. Theory Techn.*, vol. 53, no. 1, pp. 66–73, Jan. 2005.
[15] D. Deslandes and K. Wu, "Single-substrate integration technique of planar circuits and waveguide filters," *IEEE Trans. Microw. Theory Techn.*, vol. 51, no. 2, pp. 593–596, Feb. 2003.
[16] D. Deslandes and K. Wu, "Accurate modeling, wave mechanisms, and design considerations of a substrate integrated waveguide," *IEEE Trans. Microw. Theory Techn.*, vol. 54, no. 6, pp. 2516–2526, Jun. 2006.
[17] U. Naeem, A. Iqbal, M. F. Shafique, and S. Bila, "Efficient design methodology for a complex DRA-SIW filter-antenna subsystem," *Int. J. Antennas Propag.*, vol. 2017, pp. 1–9, Jan. 2017.
[18] K. Wu, "Towards system-on-substrate approach for future millimeter-wave and photonic wireless applications," in *Proc. Asia–Pacific Microw. Conf.*, Dec. 2006, pp. 1895–1900.
[19] A. Iqbal, M. A. Selmi, L. F. Abdulrazak, O. A. Saraereh, N. K. Mallat, and A. Smida, "A compact substrate integrated waveguide cavity-backed self-triplexing antenna," *IEEE Trans. Circuits Syst. II, Exp. Briefs*, vol. 67, no. 11, pp. 2362–2366, Nov. 2020.
[20] K. Kumar and S. Dwari, "Substrate integrated waveguide cavity-backed self-triplexing slot antenna," *IEEE Antennas Wireless Propag. Lett.*, vol. 16, pp. 3249–3252, 2017.
[21] A. Iqbal, J. J. Tiang, C. K. Lee, N. K. Mallat, and S. W. Wong, "Dual-band half mode substrate integrated waveguide filter with independently tunable bands," *IEEE Trans. Circuits Syst. II, Exp. Briefs*, vol. 67, no. 2, pp. 285–289, Feb. 2020.

[22] A. Iqbal, A. W. Ahmad, A. Smida, and N. K. Mallat, "Tunable SIW bandpass filters with improved upper stopband performance," *IEEE Trans. Circuits Syst. II, Exp. Briefs*, vol. 67, no. 7, pp. 1194–1198, Jul. 2020.
[23] J.-X. Chen, W. Hong, Z.-C. Hao, H. Li, and K. Wu, "Development of a low cost microwave mixer using a broad-band substrate integrated waveguide (SIW) coupler," *IEEE Microw. Wireless Compon. Lett.*, vol. 16, no. 2, pp. 84–86, Feb. 2006.
[24] A. Iqbal, J. J. Tiang, C. K. Lee, and B. M. Lee, "Tunable substrate integrated waveguide diplexer with high isolation and wide stopband," *IEEE Microw. Wireless Compon. Lett.*, vol. 29, no. 7, pp. 456–458, Jul. 2019.
[25] Y. Dong and T. Itoh, "Substrate integrated waveguide loaded by complementary split-ring resonators for miniaturized diplexer design," *IEEE Microw. Wireless Compon. Lett.*, vol. 21, no. 1, pp. 10–12, Jan. 2011.
[26] C. Zhong, J. Xu, Z. Yu, and Y. Zhu, "Ka-band substrate integrated waveguide gunn oscillator," *IEEE Microw. Wireless Compon. Lett.*, vol. 18, no. 7, pp. 461–463, Jul. 2008.
[27] Y. Cassivi and K. Wu, "Low cost microwave oscillator using substrate integrated waveguide cavity," *IEEE Microw. Wireless Compon. Lett.*, vol. 13, no. 2, pp. 48–50, Feb. 2003.
[28] W. D'Orazio and K. Wu, "Substrate-integrated-waveguide circulators suitable for millimeter-wave integration," *IEEE Trans. Microw. Theory Techn.*, vol. 54, no. 10, pp. 3675–3680, Oct. 2006.
[29] J. Hirokawa and M. Ando, "Efficiency of 76-GHz post-wall waveguide-fed parallel-plate slot arrays," *IEEE Trans. Antennas Propag.*, vol. 48, no. 11, pp. 1742–1745, 2000.
[30] S. Tae Choi, K. Seok Yang, K. Tokuda, and Y. Hoon Kim, "A V-band planar narrow bandpass filter using a new type integrated waveguide transition," *IEEE Microw. Wireless Compon. Lett.*, vol. 14, no. 12, pp. 545–547, Dec. 2004.
[31] D. Stephens, P. R. Young, and I. D. Robertson, "Millimeter-wave substrate integrated waveguides and filters in photoimageable thick-film technology," *IEEE Trans. Microw. Theory Techn.*, vol. 53, no. 12, pp. 3832–3838, Dec. 2005.
[32] E. Moldovan, R. G. Bosisio, and K. Wu, "W-band multiport substrate-integrated waveguide circuits," *IEEE Trans. Microw. Theory Techn.*, vol. 54, no. 2, pp. 625–632, Feb. 2006.
[33] Y. Cassivi, L. Perregrini, P. Arcioni, M. Bressan, K. Wu, and G. Conciauro, "Dispersion characteristics of substrate integrated rectangular waveguide," *IEEE Microw. Wireless Compon. Lett.*, vol. 12, no. 9, pp. 333–335, Sep. 2002.
[34] W. Che, D. Wang, Y. L. Chow, and K. Deng, "Analytical equivalence between substrate-integrated waveguide and rectangular waveguide," *IET Microw., Antennas Propag.*, vol. 2, no. 1, pp. 35–41, Feb. 2008.
[35] M. Bozzi, L. Perregrini, and K. Wu, "Modeling of conductor, dielectric, and radiation losses in substrate integrated waveguide by the boundary integral-resonant mode expansion method," *IEEE Trans. Microw. Theory Techn.*, vol. 56, no. 12, pp. 3153–3161, Dec. 2008.
[36] M. Bozzi, M. Pasian, L. Perregrini, and K. Wu, "On the losses in substrate-integrated waveguides and cavities," *Int. J. Microw. Wireless Technol.*, vol. 1, no. 5, pp. 395–401, Oct. 2009.
[37] X.-P. Chen and K. Wu, "Substrate integrated waveguide filter: Basic design rules and fundamental structure features," *IEEE Microw. Mag.*, vol. 15, no. 5, pp. 108–116, Jul. 2014.
[38] M. Bozzi, D. Deslandes, P. Arcioni, L. Perregrini, K. Wu, and G. Conciauro, "Efficient analysis and experimental verification of substrate-integrated slab waveguides for wideband microwave applications," *Int. J. RF Microw. Comput.-Aided Eng.*, vol. 15, no. 3, pp. 296–306, 2005, doi: 10.1002/mmce.20085.
[39] W. Che, C. Li, P. Russer, and Y. L. Chow, "Propagation and band broadening effect of planar integrated ridged waveguide in multilayer dielectric substrates," in *IEEE MTT-S Int. Microw. Symp. Dig.*, Jun. 2008, pp. 217–220.
[40] L. Sun, Y. Zhang, Z. Qian, D. Guan, and X. Zhong, "A compact broadband hybrid ridged SIW and GCPW coupler," in *IEEE MTT-S Int. Microw. Symp. Dig.*, Jul. 2016, pp. 1–3.
[41] M. Bozzi, S. A. Winkler, and K. Wu, "Broadband and compact ridge substrate-integrated waveguides," *IET Microw., Antennas Propag.*, vol. 4, no. 11, pp. 1965–1973, 2010.
[42] U. Naeem and S. Bila, "Compact SIW based multimode filters for future generation wireless front-ends," in *Proc. Eur. Microw. Conf. (EuMC)*, Sep. 2015, pp. 967–970.
[43] L. Wu, "Substrate integrated waveguide antenna applications," Ph.D. dissertation, School Eng. Digit. Arts, Univ. Kent, Canterbury, U.K., 2015. [Online]. Available: https://kar.kent.ac.uk/50526/
[44] Y. Ding and K. Wu, "Miniaturized hybrid ring circuits using T-type folded substrate integrated waveguide (TFSIW)," in *IEEE MTT-S Int. Microw. Symp. Dig.*, Jun. 2009, pp. 705–708.
[45] H.-Y. Chien, T.-M. Shen, T.-Y. Huang, W.-H. Wang, and R.-B. Wu, "Miniaturized bandpass filters with double-folded substrate integrated waveguide resonators in LTCC," *IEEE Trans. Microw. Theory Techn.*, vol. 57, no. 7, pp. 1774–1782, Jul. 2009.
[46] C. A. Zhang, Y. J. Cheng, and Y. Fan, "Quadri-folded substrate integrated waveguide cavity and its miniaturized bandpass filter applications," *Prog. Electromagn. Res. C*, vol. 23, pp. 1–14, 2011.
[47] S. Moitra and P. S. Bhowmik, "Modelling and analysis of substrate integrated waveguide (SIW) and half-mode SIW (HMSIW) band-pass filter using reactive longitudinal periodic structures," *AEU-Int. J. Electron. Commun.*, vol. 70, no. 12, pp. 1593–1600, Dec. 2016.
[48] L. Riaz, U. Naeem, and M. F. Shafique, "Miniaturization of SIW cavity filters through stub loading," *IEEE Microw. Wireless Compon. Lett.*, vol. 26, no. 12, pp. 981–983, Dec. 2016.
[49] A. Iqbal, A. W. Ahmad, A. Smida, and N. K. Mallat, "Tunable SIW bandpass filters with improved upper stopband performance," *IEEE Trans. Circuits Syst. II, Exp. Briefs*, vol. 67, no. 7, pp. 1194–1198, Jul. 2020.
[50] L.-N. Chen, Y.-C. Jiao, Z. Zhang, and F.-S. Zhang, "Miniaturized substrate integrated waveguide dual-mode filters loaded by a series of cross-slot structures," *Prog. Electromagn. Res. C*, vol. 29, pp. 29–39, 2012.
[51] A. Pourghorban Saghati, A. Pourghorban Saghati, and K. Entesari, "Ultra-miniature SIW cavity resonators and filters," *IEEE Trans. Microw. Theory Techn.*, vol. 63, no. 12, pp. 4329–4340, Dec. 2015.
[52] A. N. Alkhafaji, A. J. Salim, and J. K. Ali, "Compact substrate integrated waveguide BPF for wideband communication applications," in *Proc. Prog. Electromagn. Res. Symp. (PIERS)*, Prague, Czech Republic, Jul. 2015, pp. 135–139.
[53] H. Zhang, W. Kang, and W. Wu, "Miniaturized dual-band SIW filters using E-shaped slotlines with controllable center frequencies," *IEEE Microw. Wireless Compon. Lett.*, vol. 28, no. 4, pp. 311–313, Apr. 2018.
[54] H. Xia and Z. Xu, "Miniaturized multilayer dual-mode substrate integrated waveguide filter with multiple transmission zeros," *Prog. Electromagn. Res.*, vol. 139, pp. 627–642, 2013.
[55] L.-N. Chen, Y.-C. Jiao, Z. Zhang, F.-S. Zhang, and Y.-Y. Chen, "Miniaturized dual-mode substrate integrated waveguide (SIW) band-pass filters loaded by double/single T-shaped structures," *Prog. Electromagn. Res. Lett.*, vol. 29, pp. 65–74, 2012.
[56] A. Niembro-Martí, V. Nasserddine, E. Pistono, H. Issa, A.-L. Franc, T.-P. Vuong, and P. Ferrari, "Slow-wave substrate integrated waveguide," *IEEE Trans. Microw. Theory Techn.*, vol. 62, no. 8, pp. 1625–1633, Aug. 2014.
[57] A. Parameswaran, P. Athira, and S. Raghavan, "Miniaturizing SIW filters with slow wave technique," *AEU-Int. J. Electron. Commun.*, vol. 84, pp. 360–365, Feb. 2018.
[58] M. Bertrand, Z. Liu, E. Pistono, D. Kaddour, and P. Ferrari, "A compact slow-wave substrate integrated waveguide cavity filter," in *IEEE MTT-S Int. Microw. Symp. Dig.*, May 2015, pp. 1–3.
[59] M. Bertrand, E. Pistono, D. Kaddour, V. Puyal, and P. Ferrari, "A filter synthesis procedure for slow wave substrate-integrated waveguide based on a distribution of blind via holes," *IEEE Trans. Microw. Theory Techn.*, vol. 66, no. 6, pp. 3019–3027, Jun. 2018.
[60] J. M. George and S. Raghavan, "A design of miniaturized SIW-based band-pass cavity filter," in *Proc. Int. Conf. Commun. Signal Process. (ICCSP)*, Apr. 2017, pp. 0622–0624.
[61] B. Zarghooni and T. A. Denidni, "New compact metamaterial unit-cell using SIR technique," *IEEE Microw. Wireless Compon. Lett.*, vol. 24, no. 5, pp. 315–317, May 2014.
[62] B. Zarghooni, A. Dadgarpour, and T. A. Denidni, "Effect of stepped-impedance resonators on rectangular metamaterial unit cells," *Int. J. RF Microw. Comput.-Aided Eng.*, vol. 25, no. 7, pp. 582–590, Sep. 2015.
[63] M. Danaeian, "Miniaturized half-mode substrate integrated waveguide diplexer based on SIR–CSRR unit-cell," *Anal. Integr. Circuits Signal Process.*, vol. 102, pp. 555–561, Sep. 2019.
[64] Y. M. Huang, G. Wang, W. Jiang, T. Huang, and Z. Shao, "Half-mode substrate integrated waveguide bandpass filter loaded with horizontal–asymmetrical stepped-impedance complementary split-ring resonators," *Electron. Lett.*, vol. 52, no. 12, pp. 1034–1036, Jun. 2016.
[65] M. Danaeian, K. Afrooz, and A. Hakimi, "Miniaturization of substrate integrated waveguide filters using novel compact metamaterial unit-cells based on SIR technique," *AEU-Int. J. Electron. Commun.*, vol. 84, pp. 62–73, Feb. 2018.
[66] M. Danaeian and K. Afrooz, "Compact metamaterial unit-cell based on stepped-impedance resonator technique and its application to miniaturize substrate integrated waveguide filter and diplexer," *Int. J. RF Microw. Comput.-Aided Eng.*, vol. 29, no. 2, Feb. 2019, Art. no. e21537.

[67] B. Yin, Z. Lin, H. Hao, W. Luo, and W. Huang, "Miniaturized HMSIW bandpass filter based on the coupling of dual-iris with nested stepped-impedance CSRRS," *Prog. Electromagn. Res. Lett.*, vol. 84, pp. 115–121, 2019.
[68] T. Yang, P.-L. Chi, R. Xu, and W. Lin, "Folded substrate integrated waveguide based composite right/left-handed transmission line and its application to partial H-plane filters," *IEEE Trans. Microw. Theory Techn.*, vol. 61, no. 2, pp. 789–799, Feb. 2013.
[69] V. G. Veselago, "The electrodynamics of substances with simultaneously negative values of 'ϵ and μ,'" *Physics-Uspekhi*, vol. 10, no. 4, pp. 509–514, 1968.
[70] J. B. Pendry, A. Holden, D. Robbins, and W. Stewart, "Low frequency plasmons in thin-wire structures," *J. Phys., Condens. Matter*, vol. 10, no. 22, p. 4785, 1998.
[71] K. G. Balmain and G. V. Eleftheriades, *Negative-Refraction Metamaterials: Fundamental Principles and Applications*. Hoboken, NJ, USA: Wiley, 2005.
[72] Y. Dong and T. Itoh, "Substrate integrated waveguide negativeorder resonances and their applications," *IET Microw., Antennas Propag.*, vol. 4, no. 8, pp. 1081–1091, 2010.
[73] S. Hu, Y. Gao, X. Zhang, and B. Zhou, "Design of a compact 5.7-5.9 GHz filter based on CRLH resonator units," *Prog. Electromagn. Res. Lett.*, vol. 89, pp. 141–149, 2020.
[74] S. Hu, Y. Hu, H. Zheng, W. Zhu, Y. Gao, and X. Zhang, "A compact 3.3–3.5 GHz filter based on modified composite right-/left-handed resonator units," *Electronics*, vol. 9, no. 1, p. 1, Dec. 2019.
[75] Y.-N. Yang, G. H. Li, L. Sun, W. Yang, and X. Yang, "Design of compact bandpass filters using sixteenth mode and thirty-second mode SIW cavities," *Prog. Electromagn. Res. Lett.*, vol. 75, pp. 61–66, 2018.
[76] A. Iqbal, J. J. Tiang, C. K. Lee, N. K. Mallat, and S. W. Wong, "Dual-band half mode substrate integrated waveguide filter with independently tunable bands," *IEEE Trans. Circuits Syst. II, Exp. Briefs*, vol. 67, no. 2, pp. 285–289, Feb. 2020.
[77] B. You, L. Chen, and G. Luo, "The novel reconfigurable double-layer half-mode SIW filter with tunable DMS structure," *J. Electromagn. Waves Appl.*, vol. 32, no. 14, pp. 1816–1823, Sep. 2018.
[78] X. Nie and W. Hong, "Miniaturised QMSIW filter using comb line with high out-of-band rejection," *Electron. Lett.*, vol. 53, no. 12, pp. 785–787, Jun. 2017.
[79] Y.-D. Wu, G. H. Li, W. Yang, and X. Yang, "Design of compact wideband QMSIW band-pass filter with improved stopband," *Prog. Electromagn. Res. Lett.*, vol. 65, pp. 75–79, 2017.
[80] L. Li, Z. Wu, K. Yang, X. Lai, and Z. Lei, "A novel miniature single-layer eighth-mode SIW filter with improved out-of-band rejection," *IEEE Microw. Wireless Compon. Lett.*, vol. 28, no. 5, pp. 407–409, May 2018.
[81] Q. Liu, D. Zhou, D. Zhang, C. Bian, and Y. Zhang, "Ultra-compact quasi-elliptic bandpass filter based on capacitive-loaded eighth-mode SIW cavities," *Int. J. Microw. Wireless Technol.*, vol. 12, no. 2, pp. 109–115, Mar. 2020.
[82] A. R. Azad and A. Mohan, "A compact sixteenth-mode substrate integrated waveguide bandpass filter with improved out-of-band performance," *Microw. Opt. Technol. Lett.*, vol. 59, no. 7, pp. 1728–1733, Jul. 2017.
[83] P. Chen, X. Liu, L. Li, and K. Yang, "Miniaturized sixteenth-mode substrate integrated waveguide bandpass filter with helical slot lines," in *Proc. IEEE Asia–Pacific Microw. Conf. (APMC)*, Dec. 2019, pp. 1137–1139.
[84] A. R. Azad and A. Mohan, "Sixteenth-mode substrate integrated waveguide bandpass filter loaded with complementary split-ring resonator," *Electron. Lett.*, vol. 53, no. 8, pp. 546–547, Apr. 2017.

AMJAD IQBAL (Student Member, IEEE) received the degree in electrical engineering from COMSATS University Islamabad, Islamabad, Pakistan, in 2016, and the M.S. degree in electrical engineering from the Department of Electrical Engineering, CECOS University of IT and Emerging Sciences, Peshawar, Pakistan, in 2018. He is currently pursuing the Ph.D. degree with the Faculty of Engineering, Multimedia University, Cyberjaya, Malaysia. He was Laboratory Engineer with the Department of Electrical Engineering, CECOS University Islamabad from 2016 to 2018. His research interests include printed antennas, flexible antennas, implantable antennas, MIMO antennas, dielectric resonator antennas, wireless power transfer and synthesis of microwave components.

JUN JIAT TIANG received the degree in electronics engineering from Multimedia University, Malaysia, in 2004, the master's degree from the Department of Electrical and Electronics Engineering, University of Science, Malaysia, in 2006, and the Ph.D. degree in electrical, electronic and systems engineering with the National University of Malaysia, Malaysia, in 2014. He is currently as a Senior Lecturer and Researcher with the Faculty of Engineering, Multimedia University, Malaysia. His interests include antenna and propagation, microwave circuits, and smart antenna.

SEW KIN WONG (Member, IEEE) received the B.E. degree (Hons.) in electronics engineering from the University Science of Malaysia in 1995 and the M.E. and Ph.D. degrees from Multimedia University, Malaysia, in 2003 and 2012 respectively. He joined Mecomb Malaysia Sdn Bhd as a Sales Engineer in charge of technical sales, presales support, and customer training for telecommunication products, ranging from simple bit error rate tester to high end synchronous digital hierarchy test and measurement systems. In 2000, he left Mecomb Malaysia Sdn Bhd and joined Multimedia University as Assistant Lecturer, where he has been a Senior Lecturer with the Faculty of Engineering, Multimedia University, since 2003. He conducted research on radio frequency (RF) transceiver, amplifier, and mixer design. Under his research contributions, a front-end RF transceiver prototype for third generation (3G) cellular communication, a power amplifier, a low-noise amplifier, and downconversion mixer integrated circuits for ultra-wideband communication system were successfully deployed and developed. His main responsibilities include conducting undergraduate and postgraduate lectures, tutorials, and laboratory experiments, performing scientific research, supervising postgraduate research students, and carrying out faculty's administrative tasks. Since 2005, he has been conducting short courses and corporate trainings to engineering manufacturers, such as Agilent, Intel, Avago, Plexus, and Venture. To date, he has conducted more than 50 courses and trainings in the area of RF/microwave and telecommunication, such as fundamental or concept, transceiver system, measurement techniques, and verifications. He is a Professional Engineer (Ir.) registered under the Board of Engineers Malaysia.

MOHAMMAD ALIBAKHSHIKENARI (Member, IEEE) was born in Mazandaran, Iran, in 1988. He received the Ph.D. degree (Hons.) in electronic engineering from the Tor Vergata University of Rome, Italy, in 2020. He received the International Postgraduate Research (Ph.D.) Scholarship from the Italian Government in 2016 for three years. He was a recipient of two years postdoctoral research grant with the Department of Electronic Engineering, Tor Vergata University of Rome, in 2019.

In 2018, he was as a Ph.D. Visiting Researcher with the Antenna System Division, Department of Electrical Engineering, Chalmers University of Technology, Gothenburg, Sweden, for eight months. His training during the Ph.D. included a research stage in the Swedish company Gap Waves AB that is developing components in a technology. During his Ph.D. research period, he has participated in 14 international IEEE conferences over the world, where he has presented 20 articles mostly in oral presentations. During his Ph.D. studies, he received 13 grants for participating in the European Doctoral and Postdoctoral Schools on Antennas and Metamaterials organized by several European Universities and the European School of Antennas. He acts as a referee in several high reputed journals and the IEEE international conferences. His research interests include antennas and wave-propagations, phased-antenna arrays, metamaterials and metasurfaces, synthetic aperture radars, multiple-input multiple-output systems, waveguide slotted antenna

arrays, substrate integrated waveguides, impedance matching circuits, on-chip antennas, microwave components, millimeter-waves and terahertz integrated circuits, and electromagnetic systems. The above-mentioned research lines have produced more than 90 publications on refereed-international journals, presentations within international-conferences, and book chapters with a total number of the citations more than 1250, H-index of 25, and I10-index of 45 reported by the Google Scholar Citation. He was a recipient of the 47th and the 48th European Microwave Conference Young Engineer Prize, in 2017, Nuremberg, Germany, and in 2018, Madrid, Spain, respectively, where he has presented his articles. On 2019, he gave an invited lecture ''Metamaterial Applications to Antenna Systems'' at the Department of Information and Telecommunication Engineering, Incheon National University, Incheon, South Korea, which was in conjunction with the 8th Asia–Pacific Conference on Antennas and Propagation, where he was also the Chair of the Metamaterial Session. He is serving as an Associate Editor for *IET Journal of Engineering* and the *International Journal of Electrical and Computer Engineering*, an Section Editor for the *International Journal of Sensors Wireless Communications and Control* and the *HighTech and Innovation Journal*, and a Guest Editor for a special issue entitled *Millimeter-wave and Terahertz Applications of Metamaterials* in *Applied Sciences*. In 2020, his article ''High-Gain Metasurface in Polyimide On-Chip Antenna Based on CRLH-TL for Sub Terahertz Integrated Circuits'' published in *Scientific Reports* received the Best Month Article Award at the University of Bradford, U.K.

FRANCISCO FALCONE (Senior Member, IEEE) received the degree in telecommunication engineering and the Ph.D. degree in communication engineering from the Universidad Pública de Navarra (UPNA), Spain, in 1999 and 2005, respectively. From 1999 to 2000, he was a Microwave Commissioning Engineer with Siemens-Italtel, deploying microwave access systems. From 2000 to 2008, he was a Radio Access Engineer with Telefónica Móviles, performing radio network planning and optimization tasks in mobile network deployment. In 2009, he was the Director of Tafco Metawireless, a spin-off company from UPNA, as a Co-Founding Member, until 2009. In parallel, he was an Assistant Lecturer with the Department of Electrical and Electronic Engineering Department, UPNA, from 2003 to 2009, where he became an Associate Professor in 2009 and was the Department Head from 2012 to 2018. In 2018, he was a Visiting Professor with the Kuwait College of Science and Technology, Kuwait. He is also with the Institute for Smart Cities, UPNA, which hosts around 140 researchers. He is currently the Head of the ICT Section. His research interests are related to computational electromagnetics applied to the analysis of complex electromagnetic scenarios, with a focus on the analysis, design, and implementation of heterogeneous wireless networks to enable context-aware environments. He has over 500 contributions in indexed international journals, book chapters, and conference contributions. He received the CST 2003 and CST 2005 Best Paper Award, the Ph.D. Award from the Colegio Oficial de Ingenieros de Telecomunicación (COIT), in 2006, the Doctoral Award UPNA in 2010, the 1st Juan Gomez Peñalver Research Award from the Royal Academy of Engineering of Spain in 2010, the XII Talgo Innovation Award 2012, the IEEE 2014 Best Paper Award in 2014, the ECSA-3 Best Paper Award in 2016, and the ECSA-4 Best Paper Award in 2017.

ERNESTO LIMITI (Senior Member, IEEE) was a Research and Teaching Assistant with the Faculty of Engineering, Tor Vergata University of Rome, in 1991, where he was an Associate Professor in 1998 and where he has been a Full Professor of electronics since 2002. He represents the Tor Vergata University of Rome in the governing body of the Microwave Engineering Center for Space Applications, an inter-university center among several Italian Universities. He has been elected to represent the Industrial Engineering sector in the Academic Senate of the University for the period 2007–2010 and 2010–2013. He is the president of the Consortium ''Advanced Research and Engineering for Space,'' formed between the Tor Vergata University of Rome and two companies. He is the President of the Laurea and Laurea Magistrale degrees in electronic engineering with the Tor Vergata University of Rome. He is a member of the committee of the Ph.D. program in telecommunications and microelectronics with the Tor Vergata University of Rome, tutoring an average of four Ph.D. candidates per year. Regarding teaching activities, he teaches, over his institutional duties in the frame of the Corso di Laurea Magistrale in Ingegneria Elettronica, Elettronica per lo Spazio, within the master course in the Sistemi Avanzati di Comunicazione e Navigazione Satellitare. He is actively involved in research activities with many research groups, both European and Italian. He is in tight collaborations with high-tech Italian, including Selex-SI, Thales Alenia Space, Rheinmetall, Elettronica S.p.A., and Space Engineering, and foreign, including OMMIC, Siemens, and UMS companies. He has contributed to several National, including PRIN MIUR, Madess CNR, and Agenzia Spaziale Italiana, and international, including ESPRIT COSMIC, Manpower, Edge, Special Action MEPI, ESA, EUROPA, Korrigan, and RadioNet FP6 and FP7, projects as a researcher and/or as unit responsible. His research activities are focused on three main lines, all of them belonging to the microwave and millimeter-wave electronics research area. The first one is related to characterization and modeling for active and passive microwave and millimeter-wave devices. Regarding active devices, the research line is oriented to the small-signal, noise, and large signal modeling. Regarding passive devices, equivalent-circuit models have been developed for interacting discontinuities in microstrip, for typical MMIC passive components (MIM capacitors) and to waveguide/coplanar waveguide transitions analysis and design. For active devices, new methodologies have been developed for the noise characterization and the subsequent modeling, and equivalent-circuit modeling strategies have been implemented both for small and large-signal operating regimes for GaAs, GaN, SiC, Si, InP, and MESFET/HEMT devices. The second line is related to design methodologies and characterization methods for low-noise circuits. The main focus is on cryogenic amplifiers and devices. Collaborations are currently ongoing with the major radioastronomy institutes all around Europe within the frame of FP6 and FP7 programmes (RadioNet). Finally, the third line is in the analysis methods for nonlinear microwave circuits. In this line, novel analysis methods (spectral balance) are developed, together with the stability analysis of the solutions making use of traditional (harmonic balance) approaches. The above-mentioned research lines have produced more than 250 publications on refereed international journals and presentations within international conferences. He acts as a referee of the international journals of the microwave and millimetre wave electronics sector. He is on the steering committee of international conferences and workshops.